Sensors and Communications Systems

James D. Huffaker, Christopher K. Barker, David M. Brown, Donald E. Chesley, Thomas R. Clark Jr., G. Daniel Dockery, Charles L. Farthing, Khadir A. Griffith, Minhtri T. Ho, Shaun T. Hutton, Juan C. Juarez, Hedi A. Krichene, Joseph N. Mulé, Kenneth W. O'Haver, Shawn A. Phillips, Gerald F. Ricciardi, and Salvador H. Talisa

ABSTRACT

Sensors and communications systems are key components of air and missile defense systems, enabling those systems to search to long ranges; detect and track aircraft, missiles, satellites, and artillery; discriminate and identify threatening objects; and pass that information on to combat systems and weapons that act on it to defeat threats. Our adversaries' cruise and ballistic missile threat capabilities continue to evolve, making it challenging for our modern systems to perform these functions with sufficient accuracy and timeliness to maintain defense superiority.

INTRODUCTION

In this article, we describe evolving technologies being developed in both the radio frequency (RF) and electro-optics and infrared (EO/IR) regimes to address emerging air and missile defense challenges. We begin with an introduction to radar architecture advances over the last couple of decades, leading up to the current digital phased-array state of the art. We describe the advanced modeling and simulation (M&S) tools needed to characterize the performance of digital beamforming (DBF) arrays. We also present current areas of focus in EO/IR, including long-range free-space optical (FSO) communications and photonics for signal transport in RF sensor and communications systems. Equally important to the advancing RF and EO/IR technologies is the ability to measure the environment in which our state-of-the-art systems must operate and to adapt to or otherwise compensate for those conditions.

ADVANCED PHASED-ARRAY RADAR SYSTEMS

Radar Architecture Evolution

Phased-array radars have evolved significantly since their introduction in the 1960s time frame. Figure 1 depicts in block diagram form the evolution of phased-array radar architectures from initial passive analog array architectures of the 1960s and 1970s to the emerging digital array architectures of today. This architecture evolution has resulted from the requirements pull caused by continuing threat advances and the concurrent technology push resulting from new technology developments. A recent *Johns Hopkins APL Technical Digest* article examines this architecture evolution through the lens of APL's significant history of accomplishments in advanced radar development.[1] Phased-array radars were first introduced in the 1960s and 1970s to provide the rapid beamsteering needed to counter evolving air and ballistic missile threats. These early radar architectures
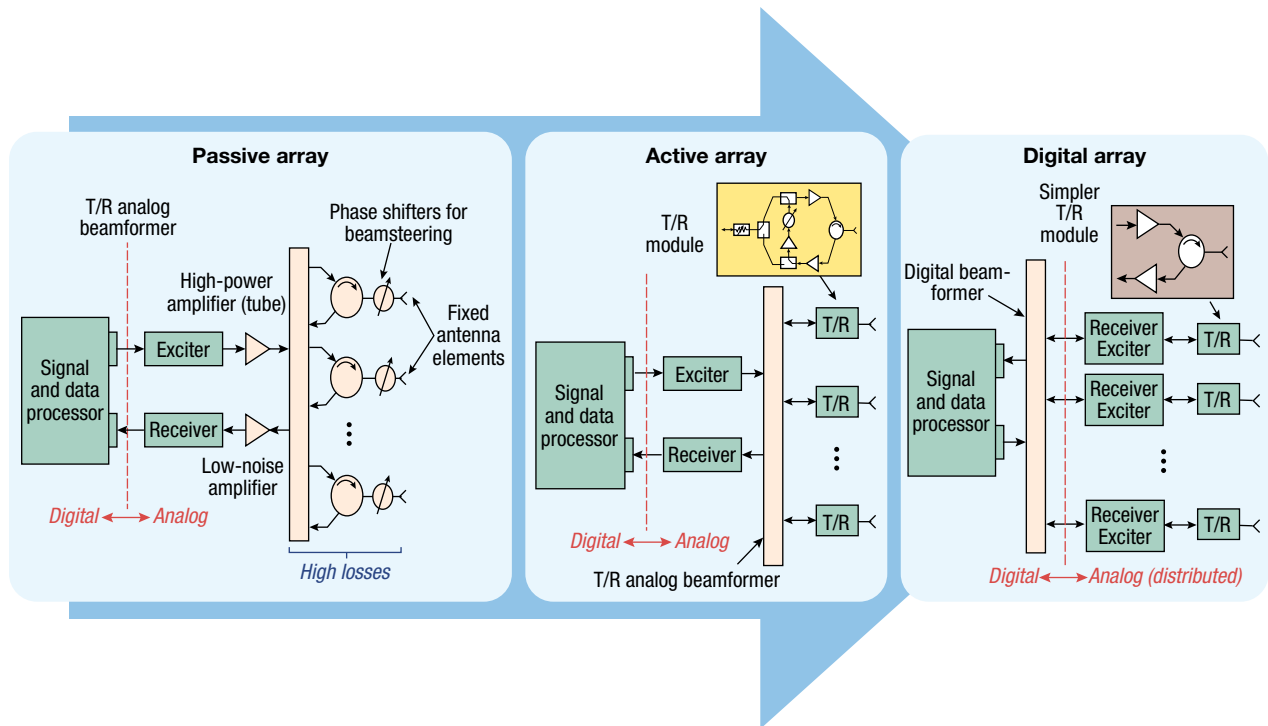
Figure 1. Evolution of radar architectures from passive analog arrays (circa the 1970s) to active electronically scanned arrays (circa the 1990s) to digital arrays (circa the 2010s). (© 2016 IEEE. Reprinted, with permission, from Ref. 2.)

featured a centralized high-power transmitter, a centralized receiver and a passive (i.e., no RF amplification) phased-array antenna. The development of practical ferrite phased shifters at APL and other laboratories provided the key enabling technology. While passive arrays introduced the attributes of electronic beamforming and improved pattern (sidelobe) control, this architecture generally required high-power transmit array beamformers and complex monopulse receive beamformers, and suffered from high transmit and receive losses. In the 1990s, the development of gallium arsenide (GaAs)-based monolithic microwave integrated circuit (MMIC) technology enabled the development of active arrays, otherwise known active electronically scanned arrays (AESAs). This architecture effectively moved transmit high-power amplification and receive low-noise amplification to the array elements in the form of the MMIC-based transmit/receive (T/R) module. The resulting benefits included significantly reduced transmit and receive losses; transition to higher-duty-factor solid-state transmission; improved system reliability; and generally reduced size, weight, and power as the centralized high-power transmitter was no longer required. More recently, with the march of Moore's law and the associated advances in RF integrated circuit technology, digital receiver and waveform generation functions can now be distributed across the array either as element-level or subarray-level digital arrays. Digital array radars enable digital beamforming and the opportunity for

significant system benefits, including multiple simultaneous beams, advanced signal processing algorithms, enhanced commonality and scalability, and realization of more software-definable array systems. Ref. 2 provides an overview of APL research into the benefits of digital-phased array radars.

Digital Array Radar Development Activities

APL has been at the forefront of digital array radar development with involvement in multiple research and development programs. These activities include the Advanced Radar Technology Integrated System Test-

Figure 2. UK and US ARTIST research radars at Wallops Island, Virginia. The radars were placed at heights representative of potential locations on UK and US Navy ships.

bed (ARTIST) and Australian United States Phased Array Radar (AUSPAR) international cooperative programs, the Defense Advanced Research Projects Agency (DARPA) Arrays at Commercial Timescales program,[3] and internal research and development. The ARTIST and AUSPAR programs are briefly described here.

ARTIST was a digital array technology risk-reduction program carried out jointly between the US and UK Navies between 2003 and 2010. Two ~1000-element, subarray-level digital array research radars were developed in the United States and in the United Kingdom, respectively, as part of the program. These radars were tested at the US Navy's Surface Combat Systems Center land-based test site in Wallops Island, Virginia (Figure 2). APL participated as government technical lead for the US ARTIST system and in the overall test direction for the project.

The two radars were developed using different approaches to subarray-level digital arrays. A number of benefits for both navies resulted from this effort, especially those derived from the testing and performance comparison between the two radars. The effort provided significant insight into and understanding of the benefits of digital arrays and advanced the state of the art in both countries.

AUSPAR (Figure 3) was a digital array technology risk-reduction program carried out jointly between the US and Australian governments between 2005 and 2015. APL participated in US efforts to define and conduct testing and evaluation as well as data collection using an element-level digital array research radar developed by CEA Technologies in Canberra, Australia. Testing verified digital array scaling of dynamic range and phase noise and demonstrated the ease of array sizing scalability and reconfigurability. The AUSPAR array was

Figure 3. AUSPAR element-level digital array under test.

brought to the United States to support development of planar near-field test techniques for digital arrays.[4] The AUSPAR array was configured to extract element-level receive data during radar operation, and this capability was used to perform data collects for test scenarios using live targets. A significant advantage of an element-level digital array is that data collected in this fashion can be processed offline in order to research and develop new radar signal-processing algorithms. Element-level receive data were collected for several scenarios, including multiple aircraft targets with and without injected jamming and pulsed interferers, multiple surface targets, and targets in various multipath environments. The AUSPAR effort demonstrated the benefits of highly flexible and relatively low-cost element-level digital arrays.

M&S FOR DIGITAL PHASED-ARRAY RADARS

At APL, we are often assigned the role of evaluating novel phased-array radar designs to assess expected performance and to address critical design challenges. Because of the complexity of modeling the phased array in the presence of both systematic and random
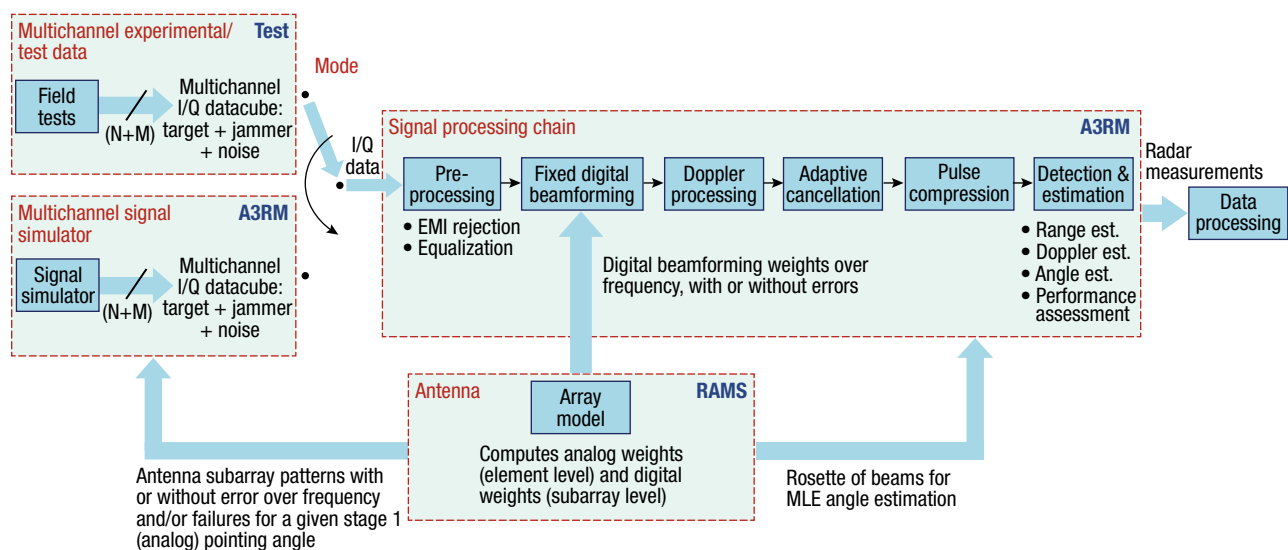

Figure 4. Block diagram of the A3RM/RAMS suite, showing the phased-array model, multichannel signal simulator, and the signal-processing chain. EMI, electromagnetic interference.

errors, performance evaluation using analytical methods is not fully descriptive, and we must rely on Monte Carlo simulations to statistically evaluate performance. Here, we describe a suite of APL-developed simulation tools that enable the modeling of complex phased-array designs at the in-phase/quadrature (I/Q) level and the statistical evaluation of their key performance metrics. A block diagram of the APL Adaptive Array Radar Model (A3RM)/Rapid Array Modeling Software (RAMS) is shown in Figure 4. The developed tools are general enough to address element-level beamforming as described in the previous section of this article, as well as analog/DBF hybrids. Novel algorithms for narrowband (NB) range estimation[5] and for the application of compressive sensing to wideband (WB) stretch processing[6] were developed at APL using the A3RM/RAMS suite of tools. Ref. 7 expands on our WB stretch processing work and develops a robust algorithm that solves the grid mismatch problem. This improved algorithm has the potential to significantly reduce the bandwidth needed to attain the same high range resolution.

Rapid Array Modeling Software

RAMS simulates the NB/WB pattern performance of very large planar phased arrays of various geometries and subarray architectures (overlapped and contiguous), all while subject to a variety of error sources that are introduced at various points in the analog and DBF chains. These include residual errors following calibration, phase shifter quantization errors, time delay control synchronization errors, element failures, and array deformation. RAMS has found, and continues to find, usage in pattern analysis, radar cross section and signature analysis, array testing, and surface deformation, as well as other integrated applications.

RAMS maintains coherency between frequencies with respect to a user-defined phase reference point to facilitate modeling of WB patterns. Closed-form solutions of the WB radiation patterns are not tractable given the tapers (and aperture weightings) under consideration, as well as the statistical errors that need to be modeled. Consequently, we resort to numerical solutions that require many transcendental functions to be evaluated at the expense of increased computation time, especially in the cases of very large planar arrays. In the case of a uniform grid with no positional errors, RAMS leverages Fourier transform theorems and the fast Fourier transform, combined with higher-order interpolation, to significantly accelerate calculations. If the effects of positional errors of the aperture elements are to be modeled, a single key subroutine has been mapped to a graphics processing unit to exploit multithreaded parallel processing and significantly reduce processing run times.[8]

RAMS either generates radiation patterns from canonical aperture distributions (e.g., uniform, Taylor,

or Bayliss weightings—useful for monopulse angle-of-arrival estimation analysis) or accepts externally generated weights, which can be computed offline using optimization techniques. By adjusting the digital weights at the subarrays, RAMS can also digitally offset a cluster surrounding the primary beam to determine the target's angle of arrival using maximum likelihood estimation (MLE), which is an alternative approach to monopulse. RAMS can also model the effects of the radiation from the element on the phased array pattern. These effects contribute to scan loss and affect polarization performance. To represent the element radiation pattern, RAMS provides the choice of using a theoretical $\cos^q(x)$ function, externally generated element-level radiation pattern data from a computational electromagnetic modeling tool such as high-frequency structure simulator (HFSS), or measured antenna data.

Fixed-Weight DBF—WB Pattern

The fixed-weight DBF capability provided by RAMS applies various analog and digital tapers to obtain low sidelobe level (SLL) performance. One important application of this capability is the generation of WB radiation patterns, which are used to verify WB SLL performance of a given array design. An example generic phased array with a 3:1 overlapping ratio in both the row and column dimensions is depicted in Figure 5, where the diamonds, green dots, and red dots denote subarray centers, elements, and single-element auxiliary channels, respectively. Subarray overlapping reduces the otherwise high sidelobes that result from subarray dispersion and grating lobe generation. This example phased-array configu-
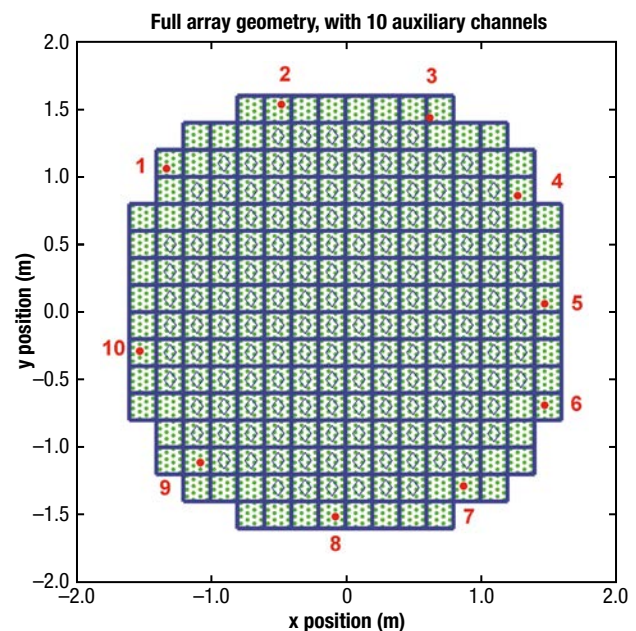

Figure 5. Example planar phased array with 3:1 overlapping ratio in both row and column dimensions.

WB radiation pattern, ρ = 3:1
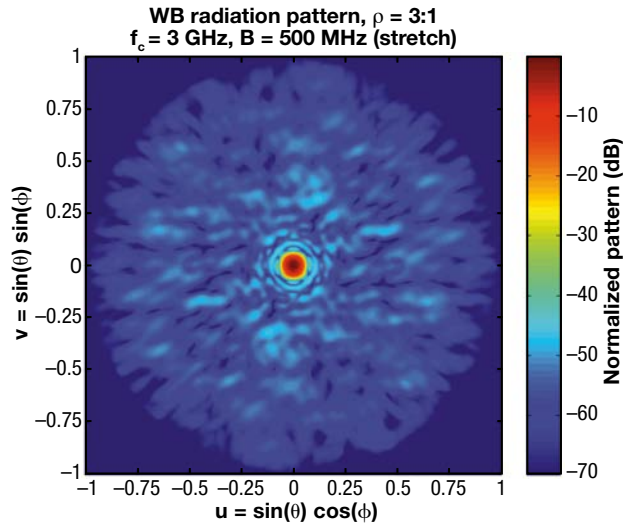**f_c = 3 GHz, B = 500 MHz (stretch)**

Figure 6. WB radiation pattern generated using stretch processing (the blurring effect is due to the averaging of multiple NB patterns). (© 2014 IEEE. Reprinted, with permission, from Ref. 8.)

ration contains 3584 radiating elements, 164 subarrays, and 10 auxiliary channels and forms the basis of the remaining simulation plots in the article. To generate the WB radiation pattern, we use stretch processing,[9] which provides high range resolution at low analog/ digital converter (ADC) sampling rates. The WB radiation pattern corresponding to the array in Figure 5 is shown in Figure 6 using a 500-MHz bandwidth. The blurring effect is caused by the averaging over multiple frequencies performed by the stretch processing.

Notch Synthesis Using Phase-Only Nulling

In the littoral regions (i.e., close to the shorelines), it may be desirable for a sector notch (or null) to be placed
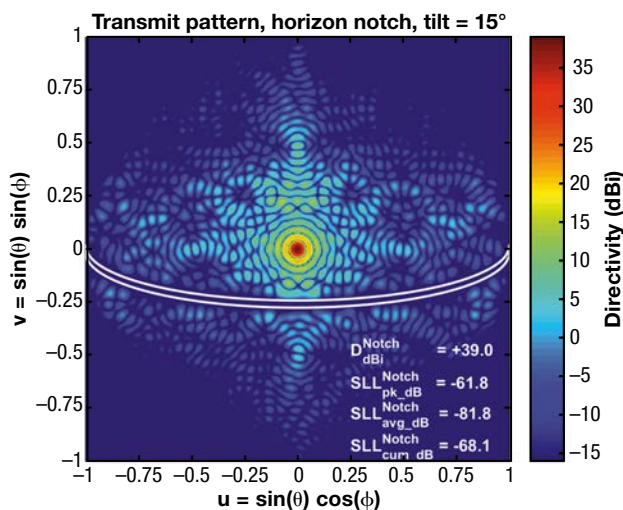

Transmit pattern, horizon notch, tilt = 15°

D_{dBi}^{Notch} = +39.0
$SLL_{pk\_dB}^{Notch}$ = −61.8
$SLL_{avg\_dB}^{Notch}$ = −81.8
$SLL_{curr\_dB}^{Notch}$ = −68.1

Figure 7. Transmit radiation pattern showing the horizon clutter notch created using the Day algorithm (the provided sidelobe metrics apply only to the notch region).

in the beam pattern on the horizon to limit illumination of discrete scatterers, to significantly reduce clutter returns, nullify radiation emanating from a known jammer location, or block electromagnetic interference signals originating from a friendly radar in the vicinity. To place a notch at a particular region in space, phase-only nulling techniques, which ensure maximum output power, can be used in both transmit and receive antenna patterns to synthesize the appropriate weights. One key example is the Day algorithm[10] developed at APL. Figure 7 shows a RAMS simulation of an ideal (i.e., no noise or errors are included) NB transmit radiation pattern that includes a horizon clutter notch of width ±1° generated using the Day algorithm and the example phased array in Figure 5. The "smile" shape of the notch is due to an assumed 15° tilt angle of the array and the nonlinear way the notch gets mapped in the antenna coordinates.

APL Adaptive Array Radar Model

A3RM models the signal-processing chain in addition to the antenna array design and provides measurements to higher-level data-processing functions. A3RM is primarily intended to assess detection performance of planar phased arrays that are divided into (possibly overlapped) subarrays for DBF, and as depicted in Figure 4, it works hand in hand with RAMS described above.

Figure 4 depicts the block diagram of A3RM, which comprises three decoupled modules: the phased array model (which uses integrated output from RAMS), the multichannel signal simulator, and the signal-processing chain. A3RM processes received data, either simulated or experimental/test, one whole coherent processing interval (CPI) at a time. The received signals from a single CPI are aggregated into a 3-D data cube whose dimensions are channel, pulse, and range. A3RM models both NB and WB waveforms at baseband using complex-valued I/Q representation. The MCSS processes the target and jammer signals through the subarray and auxiliary radiation patterns provided by RAMS, creating a matrix of received signals for each subarray and auxiliary channel (the dimensions of the matrix are pulse and range). It also models various analog components and nonideal hardware effects, which include the ADC, amplifier nonlinearities, attenuator, channel mismatch, Chebyshev filters, local oscillator phase noise, and mixing spurs. Analysis of the impacts of these signal-processing hardware effects can be found in Refs. 11 and 12.

The signal-processing chain in A3RM can perform the following I/Q processing operations on the received signals in the data cube: fixed-weight DBF, Doppler processing, adaptive jamming cancellation, pulse compression including matched filter and WB stretch processing, and detection/estimation. To remove barrage noise interference, A3RM performs sidelobe and mainlobe
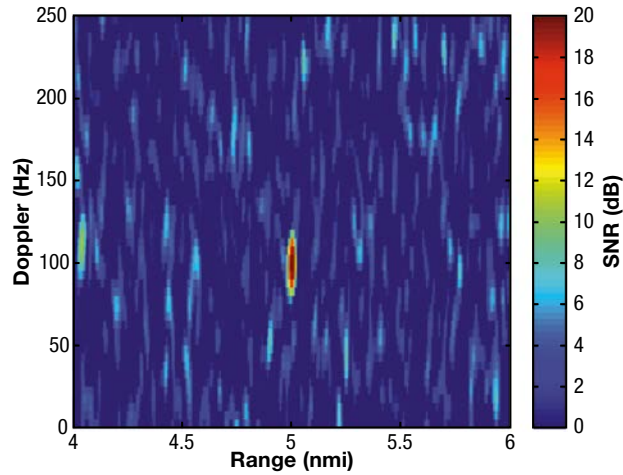
Figure 8. Example NB range-Doppler map produced by A3RM, showing a target located at 5-nmi range and 100-Hz Doppler.

jamming cancellation for both NB and WB (stretch) waveforms. Then it applies Doppler processing, pulse compression, and constant false alarm rate detection to locate the target in range, Doppler, and angle. Because adaptive beamforming uses a data-adaptive covariance matrix and is thus a nonlinear operation, the order of the signal-processing blocks in Figure 4 can be varied to evaluate the performance of different adaptive signal-processing architectures, such as pre-Doppler and post-Doppler adaptive beamforming. The only operation that must be performed last is constant false alarm rate detection. Figure 8 depicts a range-Doppler map generated by A3RM[13] for an NB target located at a range of 5 nmi and Doppler of 100 Hz in a clear (i.e., no jamming) environment. Next we discuss in detail adaptive beamforming, which is used to cancel barrage noise jamming from the sum beam.

Adaptive Beamforming

When jammers are present in the environment, fixed-weight DBF may no longer be sufficient to suppress the interference and maintain acceptable detection performance because the SLL cannot be pushed down infinitely with fixed tapers, and the residual calibration errors further limit the effects of tapers. Methods for computing data-adaptive weights that cancel jamming from the sum pattern are thus desired in order to place nulls at the

locations of the interfering signals that remain robust to the presence of residual calibration error. Depending on the spatial locations of the jammers, we can apply either sidelobe cancellation (i.e., jammers are in the sidelobes) or mainlobe cancellation (i.e., jammers are either near or in the mainlobe of the sum pattern). A sidelobe canceler (SLC) uses auxiliary channels (e.g., the elements denoted in red in Figure 5) to remove jammer signals from the sum beam of a phased array; SLC estimates the correlation statistics between the auxiliary and sum beam channels to compute the optimum cancellation weights. Mainlobe cancellation uses the same statistical techniques as those used in SLC, except that the auxiliary channels are now full array beams that are slightly offset from the radar boresight to obtain enough gain on the interfering signals. Figure 9 depicts a notional diagram of an SLC system, where the adaptive weights $\{w_M\}$ are computed to remove the jammer signals from the sum beam using the outputs of the auxiliary channels. In mainlobe cancellation, the auxiliary channels are replaced by offset sum beams, which are in effect synthetic auxiliaries.

Narrowband Jamming Cancellation

Figure 10 shows a plot of NB pulse-compressed outputs in the presence of a sidelobe jammer, using the main array and auxiliary channels shown in Figure 5. The unadapted curve shows the effect of a sidelobe jammer on a target located at 1 nmi, which becomes completely submerged in noise. After adaptive SLC processing, the target is clearly shown above the thermal noise floor. The bandwidth assumed is 10 MHz, which translates into 15-m range resolution.
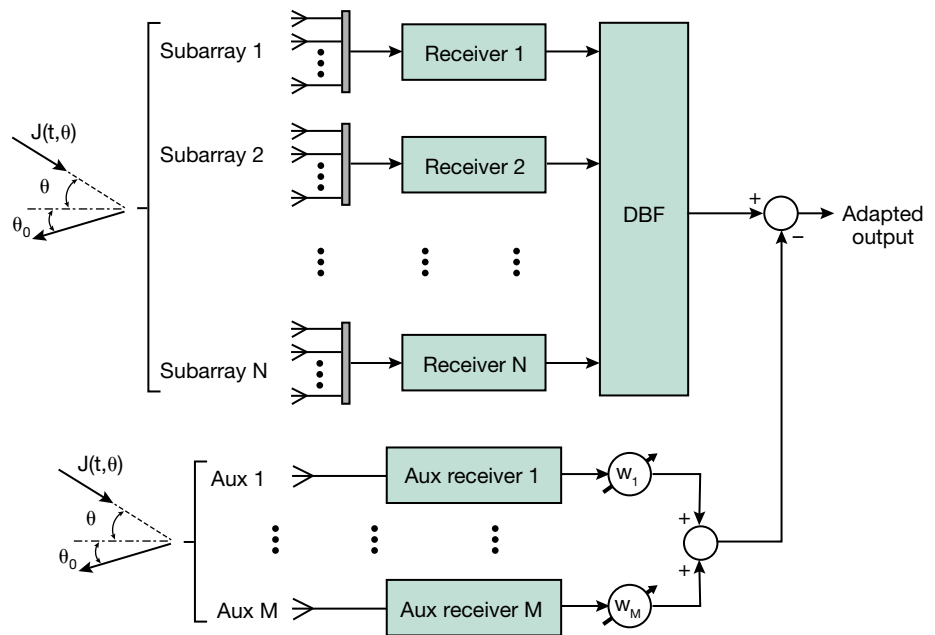

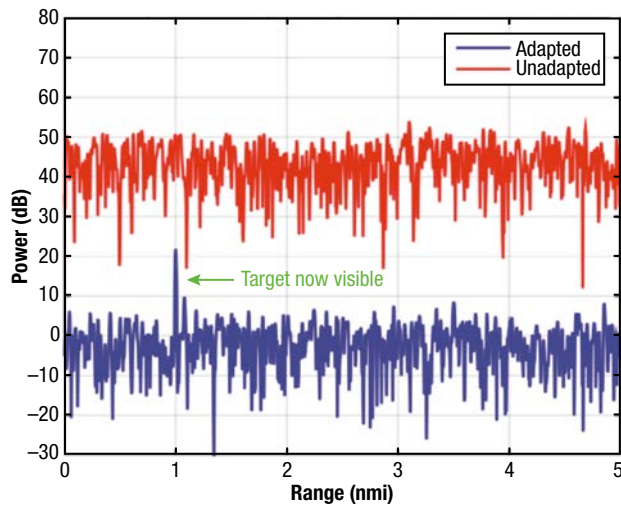**Figure 9.** Block diagram for a notional SLC system.

Figure 10. Plot of unadapted and adapted NB pulse-compressed output, clearly showing the target above the thermal noise floor after adaptive sidelobe cancellation.
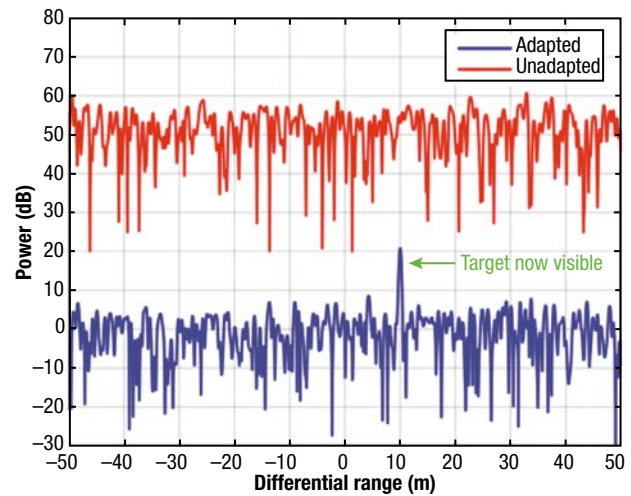

Figure 11. Plot of unadapted and adapted WB pulse-compressed output, clearly showing the target above the thermal noise floor after adaptive sidelobe cancellation.

WB Stretch Jamming Cancellation

WB pulse compression is commonly performed using stretch processing in order to use ADCs at low sampling rates. A broadband barrage noise jammer transmits energy across the band to raise the noise floor and prevent detection. WB jamming cancellation can potentially be used to cancel jammers in either the sidelobe or mainlobe regions when the instantaneous bandwidth of the radar signal is large compared with the center frequency, as is the case for stretch processing. The deramper in stretch processing renders the statistics of the jamming signal nonstationary. Performing jamming cancellation in stretch processing is problematic because the cross-correlations between the outputs of the sum beam and the auxiliary channels, and also the correlations between the auxiliary channels themselves, are time varying. Hence, standard NB techniques, which assume the statistics to be stationary, are not applicable.

In Ref. 14 we investigated, via A3RM simulation, the performance of the two major classes of algorithms that cancel sidelobe jamming in a WB phased-array radar that uses stretch processing of beamspace output. One approach for addressing the nonstationarity in statistics is to divide the stretched output into segments and apply standard NB cancellation on each segment. The other approach is to model the weight vector as inherently time varying. To each approach we also added subbanding to further decrease the nonstationarity of the stretched jammer signals and time-taps to combat dispersion across the array. We showed via simulation that when the jammers are in the sidelobe region, both approaches provide comparable performance. The subbanded variant of the segmentation-based approach was ultimately deemed the best-performing

algorithm for WB sidelobe cancellation because it is approximately eight times less complex than the time-varying approach and channelization through sub-banding aids in channel equalization. Figure 11 shows a plot of WB pulse-compressed outputs in the presence of a sidelobe jammer using the main array and auxiliary channels shown in Figure 5. The target is a single scatterer located at 10 m with respect to the reference range of the stretch processor, which is set to 0 m. The unadapted curve shows the effect of a sidelobe jammer on the target, which is completely submerged by the noise. After adaptive SLC processing using the segmentation-based method, the target is clearly shown above the thermal noise floor. We used a bandwidth of 500 MHz, which translates into a range resolution of 0.3 m. The x coordinate is labeled "differential range" because it is the difference in range between the scatterer and the reference point.

ADVANCES IN EO AND IR TECHNOLOGIES AND SYSTEMS

EO/IR technology is serving an increasingly important role in air and missile defense systems as well as many other areas in defense and commercial industries. In our diverse efforts, we seek to understand and develop EO/IR devices and systems involving the generation, transmission, detection, processing, and control of the electromagnetic spectrum from the visible through the IR as well as strategically apply the technology to defense systems operating from the RF, microwave and millimeter wave through terahertz, visible and IR.

In this section, we highlight two of our recent EO/IR technology improvement efforts in optical communications and microwave photonics.
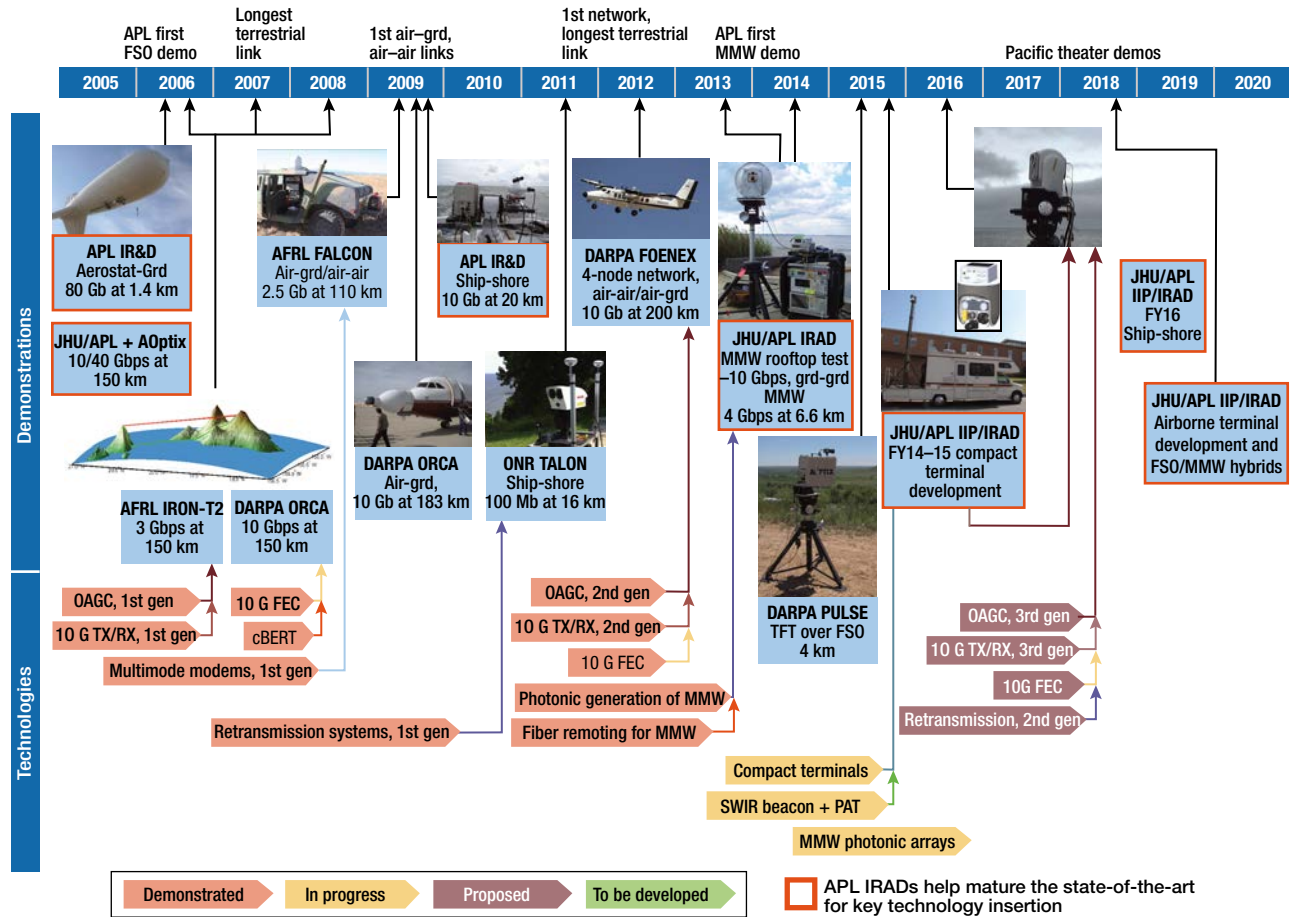
Figure 12. History of major APL demonstrations and related IRAD developments in FSO. cBERT, custom bit error rate tester; FEC, forward error correction; FOENEX, Free Space Optical Experimental Network Experiment; grd, ground; IIP, integrated investment plan; MMW, millimeter wave; OAGC, optical automatic gain control; ORCA, Optical RF Communications Adjunct; PACOM, US Pacific Command; PAT, pulse selecting pattern; SWIR, shortwave infrared; TFT, thin-film transistor.

Optical Communications: FSO Communications Technologies at APL

APL has developed and field tested a number of technologies for high-bandwidth FSO links over the last decade under activities funded by independent research and development (IRAD), the Air Force Research Laboratory (AFRL), DARPA, and the Office of Naval Research

(ONR), as illustrated in Figure 12. As part of these efforts, APL has also developed a number of technologies for characterizing data throughput and atmospheric conditions as well as high-fidelity FSO link budget models.

The longest known terrestrial FSO links were demonstrated as part of the AFRL's IRON-T2 and DARPA's Optical RF Communications Adjunct (ORCA) programs, of which APL was an integral part. The 147-km
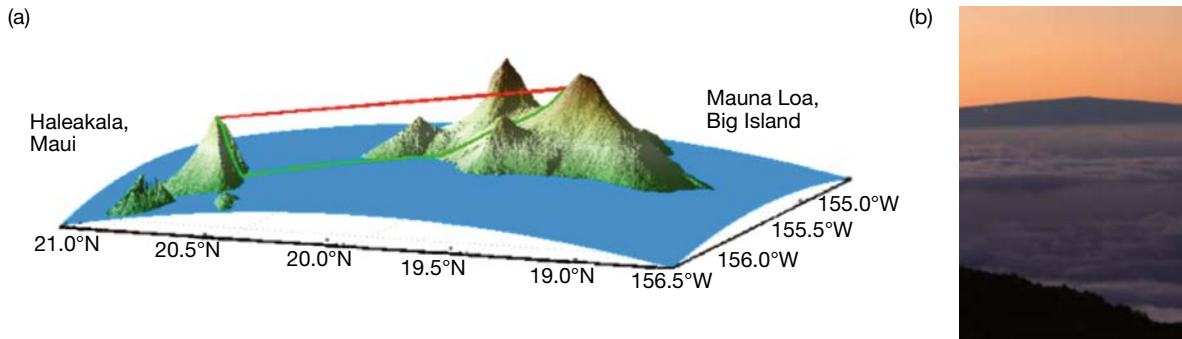

Figure 13. (a) Hawaii link test configuration in 2006, 2007, and 2008 and (b) view of Mauna Loa as seen from Maui during 2008 testing.
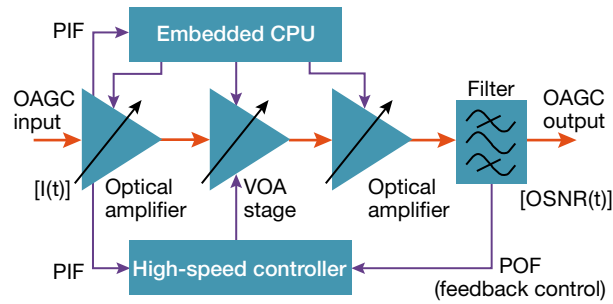
Figure 14. OAGC block diagram. CPU, central processing unit; OSNR, optical signal-to-noise ratio; PIF, power in fiber; POF, power out of the fiber; VOA, variable optical attenuator.

Figure 16. Measured DPSK transceiver and automatic gain control bit error rate baselines as a function of received optical power into the OAGC. NRZ, nonreturn to zero; RZ, return to zero.

range between the islands of Hawaii and Maui was used for FSO link testing multiple times in 2006, 2007, and 2008, as illustrated in Figure 13.

The 2006 tests, conducted by APL and AOptix Technologies, demonstrated the link for the first time during nighttime and early morning operation with single channel and wavelength division multiplexed bidirectional channels of 2.5 and 10 Gbps for aggregate data rates of up to 40 Gbps. Tests in 2007, conducted by APL with AOptix, as well as L-3 Communications Systems West, first demonstrated the optical automatic gain control (OAGC) technology developed by APL (Figures 14 and 15), enabling enhanced link sensitivity and dynamic range along with packet retransmission technologies by L-3 Communications Systems West. For both the 2006 and 2007 sets of tests, 11-in. adaptive optics systems developed by AOptix were used for the FSO terminals. The 2008 Hawaii test served as a risk-reduction effort for the DARPA ORCA flight tests of 2009. During this test, 10-Gbps forward error correction (FEC) systems and customized bit error rate testers were developed by APL for improved data throughput and link characterization capabilities, respectively. At this test, AOptix Technologies demonstrated improved performance from 4-in. adaptive optics terminal apertures, compared to the previously used 11-in. systems. This test
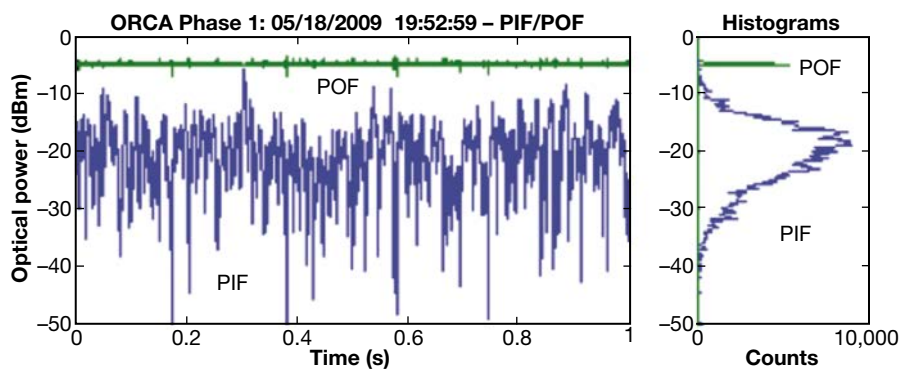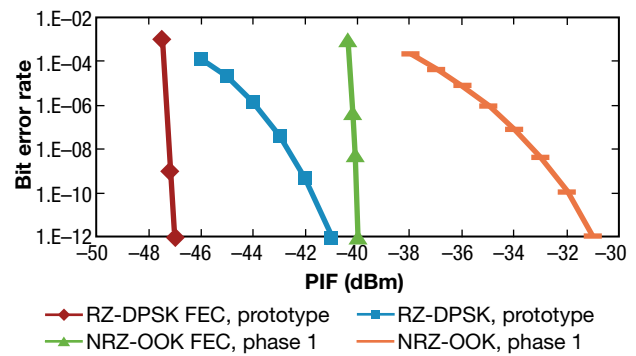
also demonstrated the first full daytime link operation during peak turbulence conditions.

Under the DARPA ORCA program, the first air-to-ground hybrid FSO/RF link was demonstrated at up to 183 km in 2009. Figure 15 presents ground power in fiber (PIF), which illustrates the dynamic nature (>40-dB swings) of the received signal at the output of the single-mode FSO terminal due to scintillation. Because commercially available high-sensitivity receivers (e.g., avalanche photodiodes) have limited dynamic ranges and suffer from saturation and damage from large power variations, the OAGC system serves as an interface between the dynamic FSO link and the photoreceiver. The OAGC accomplishes this by compensating for the dynamics in the received signal to provide a constant output while also providing low-noise optical amplification.

Additionally under the ORCA program, APL prototyped high-sensitivity, on–off keying (OOK) and differential phase shift-keying (DPSK) modems with FEC and enhanced OAGCs for improving demonstrated link sensitivities. Bit error rate baselines for these second-generation optical modems are presented in Figure 16. The DPSK waveform sensitivity of –47 dBm represented nearly an 8-dB improvement over the OOK waveform sensitivity demonstrated during the Hawaii tests, translating into significantly extended range performance in future tests.

Following the milestones demonstrated in the AFRL IRON-T2 and DARPA ORCA programs, APL was selected to lead the DARPA Free Space Optical Experimental Network Experiment (FOENEX) program. APL served as prime contractor, chief engineer, platform integrator, and optical modem developer. The developer of the networking and RF systems was L-3 Communications Systems

Figure 15. Example operation of first-generation OAGC during ORCA flight tests.

West. The FSO terminals were developed by AOptix Technologies and were based on Wescam MX15i gimbal systems.

Under this program, a hybrid FSO/RF network architecture (Figure 17) between multiple airborne and ground nodes (Figure 18) was demonstrated in 2012. During two field test phases, diamond, triangle, and string networks were demonstrated using both hybrid (FSO/RF) and FSO-only links between three aircraft and one ground station as illustrated in Figure 19. The original program metrics were to demonstrate FSO data throughputs exceeding 2.5 Gbps and RF data throughputs of greater than 200 Mbps per link. Target link distances for the air-to-ground portion of the network were to be greater than 50 km, while distances for the air-to-air link were to be greater than 200 km. All program goals for link range and data rate were exceeded with sustained error-free data transport.

After FOENEX, AOptix Technologies decided to stop supporting DoD programs to focus on their commercial efforts. Thus, to address repeated requests from operationally focused sponsors, since 2012 APL has undertaken internal development efforts to reduce the cost, size, weight, and power requirements of the FSO optical terminal. The current developmental system (Figure 20) is based on a Vector 20 inertially stabilized gimbal designed for maritime platforms. With a complete FSO payload, the final terminal weight is estimated to be ~35 lb. By leveraging the long-haul fiber communications single-mode fiber optical modem technology, the system is expected to provide FOENEX-level data rate and range performance.

Microwave Photonics: Broadband Spectrum Analysis with Photonic Compressive Sampling

Photonic technology has many advantages when applied to analog and digital signal transport systems, including low transport loss over lightweight, flexible, and electromagnetically immune cables. Photonic technology also presents a unique ability to sample, process, and distribute WB RF signals because of the availability of WB modulators and precise time bases using the short pulses of mode-locked lasers, as well as the low-loss
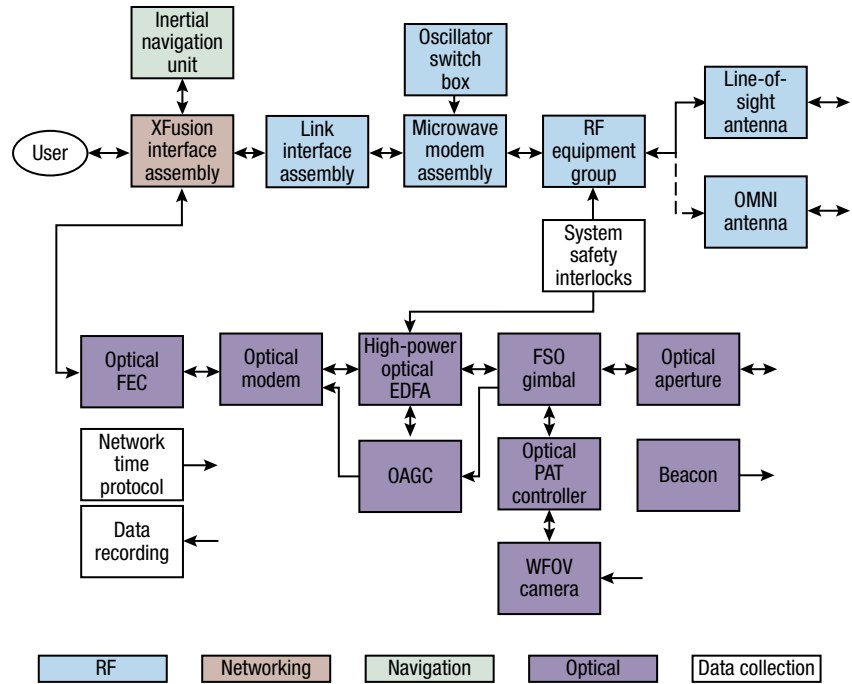

Figure 17. Block diagram of FOENEX network system. EDFA, erbium-doped fiber amplifier; OMNI, omnidirectional; PAT, pulse selecting pattern; WFOV, wide field of view.

Figure 18. FOENEX test aircraft with two optical and one RF aperture and ground station with two optical and two RF apertures.

optical fiber. These advantages have previously allowed for uniform downsampling of NB high-frequency signals digitized at high resolution.[15–17] The same benefits also make photonics attractive for pseudorandom sampling where accurate timing information is necessary to reconstruct broadband signals from nonuniform time samples.[17] The Shannon–Nyquist theorem states that a signal containing frequencies no higher than B can be completely represented by uniformly sampling the signal at a frequency $2B$. However, results of compressive sampling theory show that a large class of signals can be exactly reconstructed at average nonuniform sampling rates well below the Nyquist rate.[18–21]

In this article, we demonstrate a photonic compressive sampling ADC (PCS-ADC) to estimate the RF frequency and bandwidth of multiband signals using an average sampling rate that is more than an order of magnitude lower than the rate required by traditional Nyquist sampling.
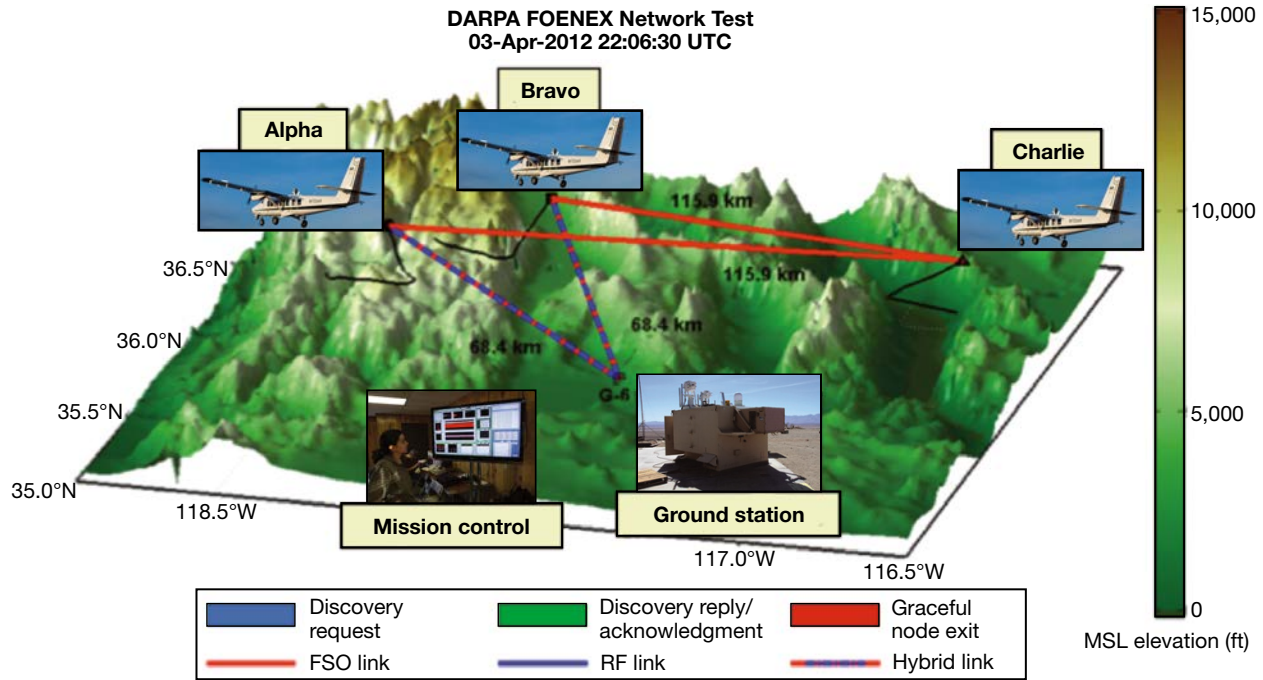
Figure 19. FOENEX network demonstration in China Lake on April 3, 2012. MSL, mean sea level.

Compressive Sampling Concept

Compressive sampling seeks to reconstruct signals with a sampling rate much lower than the Nyquist rate. In previous work, we have experimentally demonstrated a technique for achieving frequency reconstruction based on digital alias-free signal processing.[17,22] Achieving accurate reconstruction of signal bandwidth has proven difficult with this technique. One promising sampling scheme proven to handle bandwidth estimation is multicoset (MC) sampling.

This work uses a periodic nonuniform sampling technique that may be alternatively described in the framework of MC sampling.[18] Let N be the number of nonuniform samples in a period, and let f_{MC} denote the frequency at which this set of samples is repeated. In the context of MC, N is the number of cosets and f_{MC} is the MC sample rate.

In this work, all sample times are selected from a 10-GHz grid, implying a full-reconstruction bandwidth of 5 GHz. To reconstruct the sampled signal, the spectrum is divided into consecutive bins of size f_{MC}. The signal subspace is first found using a correlation approach similar to that in Ref. 21 and thresholding the eigenvalues of the resulting correlation matrix. This is followed by a greedy multiple measurement vector sparse estimation approach[23] to estimate the bins containing spectral content. Next, the signals contributing to the spectral content in each of those identified bins are estimated by a least-squares approach.

Experimental Setup

Figure 21 shows the compressive sampling ADC architecture. It consists of three main subsystems: sampling pulse generator, signal encoder, and nonuniform-to-uniform optical-to-digital converter. For sample pulse generation, the system uses an optical pulse generator (OPG) with a repetition rate of 10 GHz. Directly after the OPG, a Mach-Zehnder modulator (MZM) biased at null and driven by a pulse pattern generator serves to select individual optical pulses according to the MC sampling scheme. The downselected nonuniform pulse train is then amplified by an erbium-doped fiber amplifier (EDFA) before being split by a coupler into two identical pulse streams.

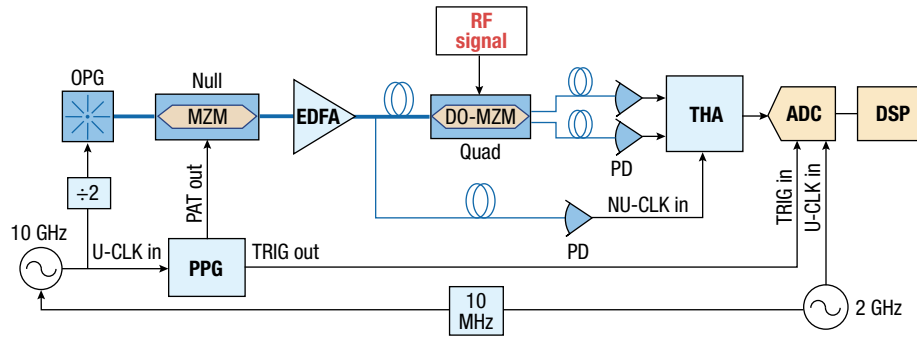**Figure 20.** APL FSO terminal prototype.

Figure 21. Photonic compressive sampling system diagram. Blue lines represent fiber, and thick blue lines are polarization maintaining. Black lines represent electrical cables. ÷2, frequency divide-by-2 circuit; DSP, digital signal processing; NU-CLK, nonuniform clock; PAT, pulse selecting pattern; PD, photodiode; PPG, pulse pattern generator; TRIG, trigger; U-CLK, uniform clock.

contributor to the front-end bandwidth of the system. The amplitude modulation of the pulse stream by the modulator is equivalent to sampling the RF waveform with the optical pulses. The primary and complementary outputs of the MZM are sent to separate PIN photodiodes, and the resulting electrical signals are used as a differential input to a track-and-hold amplifier (THA) circuit with a maximum sample rate of 2 GS/s.

The nonuniform pattern consists of 16 MC channels at a pattern repetition rate of 50 MHz (T = 20 ns). This results in a mean sampling rate f_s of 800 MHz, which can be compared to the required Nyquist sampling rate of 10 GHz for 5-GHz bandwidth reconstruction.

For signal encoding, one copy of the pulse train passes through a dual-output MZM (DO-MZM) (40-GHz bandwidth) biased at quadrature where the RF input signal modulates the pulse sequence. At this point, the pulses nonuniformly sample the RF signal. The input RF signal is in no way synchronized to the PCS-ADC architecture. The RF encoding modulator is the primary

The second copy of the nonuniform pulse train is delay-matched to the first copy and is used to nonuniformly clock the THA to ensure the circuit samples at the peak of each input pulse.

Finally, the output of the THA is sent to a single electrical ADC (3-GHz bandwidth), which is uniformly clocked at 2 GHz and phase locked to the 10-GHz OPG. A trigger signal is sent from the pulse pattern generator to the ADC at the beginning of the sequence to synchronize the capture time of the ADC. Because the MC pattern mean sampling rate of 800 MHz is not equal to the ADC sampling rate, extraneous samples of THA voltages are thrown out before signal processing. All experiments shown here use a capture time of 50 µs (100,000 ADC samples). A desktop computer (Intel Core 2 Duo, 3 GHz) implements the reconstruction algorithm and displays the reconstructed 5-GHz band with a refresh rate of approximately 1 Hz. The reconstruction itself takes approximately 20 times more computational time than a fast Fourier transform. Figure 22
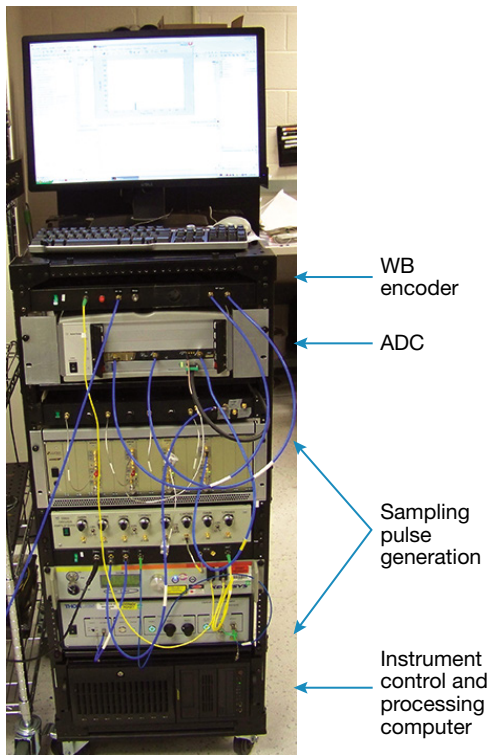

Figure 22. One-half rack PCS-ADC hardware test bed showing major subsystems.
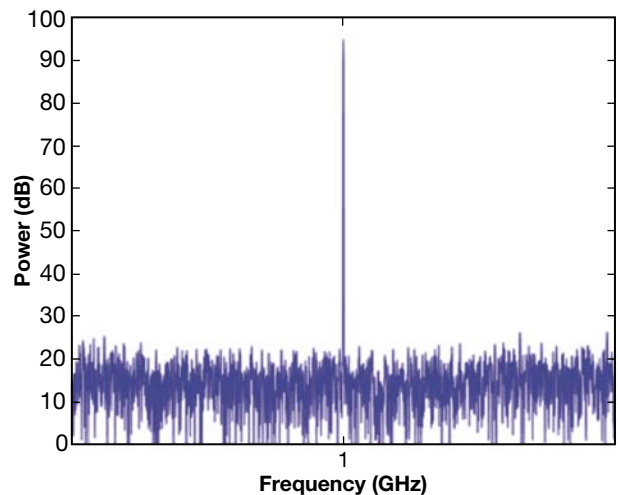

Figure 23. SNR test with a single-tone 1-GHz signal. The figure has a span of 50 MHz.

shows the complete PCS-ADC hardware test bed mounted in a one-half height, 19-in. rack.

Experimental Results

The signal-to-noise ratio (SNR) capability of the nonuniform sampling system is measured in Figure 23 with an input tone at 1 GHz at 11.6 dBm, which is the system's 1-dB compression point. The SNR is measured to be 44.7 dB with the noise power integrated across the 50-MHz reconstructed band. As mentioned above, MC reconstruction only performs reconstruction on frequency space identified as having signal, the signal subspace, so the only noise contribution for the processed output comes from the 50-MHz band containing the tone. The maximum signal-to-spur ratio (SSR) is 68.6 dB.

To demonstrate center frequency identification and bandwidth reconstruction, we use quadrature phase-shift-keying communications signals with raised cosine filtering. Panels b, d, and f in Figure 24 show the spectrum as measured by an RF spectrum analyzer for each of the individual input signals with characteristics described by Table 1. These three signals were input to the PCS-ADC simultaneously. Figure 24a shows the actual output of the compressive sampling reconstruction algorithm, which was provided information on only the signal content's band (i.e., the signals are located somewhere in the 25- to 30-GHz regime). The algorithm identified the correct three signal subspace regions to perform detailed reconstruction. Frequency and amplitude resolution have been measured to be less than 100 kHz and 0.5 dB, respectively. Panels c, e, and g in Figure 24 show zoomed-in spectral reconstruction for comparison to the known input signals. The full band of 25–30 GHz has been reconstructed without aliasing, and all center frequencies and bandwidths have been properly identified.

As a result of these efforts, we have experimentally demonstrated a WB PCS-ADC system that uses MC sampling and reconstruction. The system is capable of unambiguously identifying signals from DC to 50 GHz in a 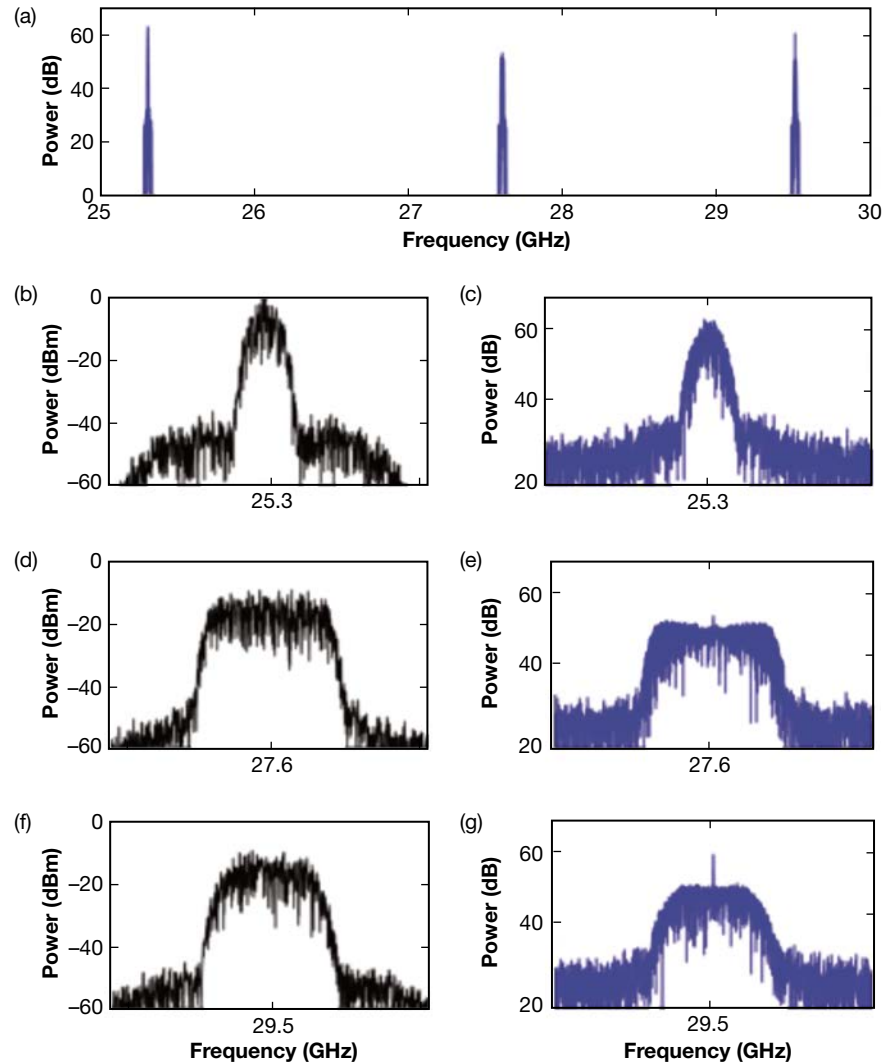5-GHz instantaneous band using an average non-uniform sample rate at 8% of the Nyquist rate. The system demonstrated high-fidelity reconstruction of multiple RF signals with bandwidth, showing correct frequency identification and spectral shape reconstruction. Amplitude-modulated carriers were reconstructed with kilohertz frequency spacing and small modulation depths. Pulsed carriers with detailed spectral features were also accurately reconstructed. In addition, the system's digital signal processing was done with low latency.

Figure 24. Spectrum analyzer trace (black) and system reconstruction (blue) of multiple communications signals. (a) The reconstructed signals in the 5-GHz instantaneous bandwidth. Panels b–g have spaces of 50 MHz and cover 60 dB of power dynamic range.

Table 1. Characteristics of communications signals used to test the system in a multisignal environment

Figure	Carrier (GHz)	Symbol Rate (MHz)	Roll-off Factor	Power (dBm)
Figure 29, b and c	25.3	10	1.0	4.1
Figure 29, d and e	27.6	24	0.2	0.4
Figure 29, f and g	29.5	22.5	0.5	−0.4

This architecture capitalizes on the strengths of photonics, namely wide bandwidth, high speed, and low jitter and amplitude noise, in order to achieve these performance capabilities.

NATURAL ENVIRONMENT MODELING FOR RADAR AND EO/IR

The natural environment can have a first-order impact on the performance of radar and EO/IR systems, particularly in a US Navy maritime environment. In this section, we describe ongoing efforts to advance the current state of the art in the measurement and modeling of effects on US Navy surface radar systems and new technologies to characterize the environment affecting EO/IR systems, including optical intelligence, surveillance, and reconnaissance; HEL (high-energy laser) engagements; and FSO communications.

Impacts on US Navy Radars

The effects of the environment on US Navy radar systems were first observed during early AN/SPY-1 field tests. Over the past three decades, APL has developed instrumentation to characterize the tropospheric propagation environment impacting these systems and physics-based M&S software that use those characterizations to help the Navy understand and predict the effect of the environment on radar systems.[24]

At low elevations (e.g., within one or two beamwidths of horizontal), the RF propagation environment has a first-order impact on the ability of a sensor to detect and track a target because of multipath, atmospheric refraction, and clutter.

At higher elevations, the primary environmental effects are signal attenuation and position measurement errors due to refraction (bending) of the radar main beam. However, clutter can still be an effect at higher elevation if it enters the system through horizon-directed antenna pattern sidelobes, particularly if in-close clutter is folded together in range with target returns for multi-pulse waveforms.

Radar returns from targets on the sea surface may be blocked or shadowed by ocean waves in addition to the refraction effects impacting low-elevation air targets. In addition, their slower speeds often make detection within the background sea clutter more difficult than for airborne targets. To capture the environmental effects that drive RF sensor performance in these cases, the effects of ocean wave blockage and scattering from the ocean surface must be coupled into the propagation factor calculations. Traditional statistical approaches are not adequate because they are designed to at best average out or, more typically, totally ignore wave blockage. Because of the small size and relatively slow speeds of surface targets, the spatial and temporal nature of sea clutter and blockage is important. In particular, the "spiky" behavior of sea clutter can cause patches of clutter to appear target-like for a short duration of time. Seas spikes can negatively impact radar systems focused on surface targets by causing false tracks or by confusing or stealing the track of a valid surface target. In addition, the plumes of water generated by ordnance aimed at these surface targets often present a target-like return that lasts for several seconds and can corrupt the track of a surface target.

Characterizing RF Propagation

RF refractivity is a characterization of the RF propagation environment and is related to meteorological parameters (temperature, pressure, and humidity) as shown in Eq. 1,

$$N(r,z) = 77.6 \frac{P(r,z)}{T(r,z)} - 5.6 \frac{e(r,z)}{T(r,z)} + 3.75 \times 10^5 \frac{e(r,z)}{T(r,z)^2}, \quad (1)$$

where (r, z) indicates the quantity is a function of range (r) and altitude above sea level (z); N is RF refractivity $\equiv (n - 1)*10^6$, where n is the refractive index of air; P is total air pressure, including partial water vapor pressure, in millibars; e is partial water vapor pressure, in millibars, which is relatable to relative humidity; and T is air temperature in Kelvin.

Analysis of Eq. 1 indicates that significant changes in N are caused by the vertical derivative dN/dz. Thus, the question of "what matters to RF propagation?" then becomes "what has the biggest effect on dN/dz?" Water vapor (de/dz) is the biggest contributor to dN/dz, followed by temperature (dT/dz) and pressure (dP/dz). As an illustrative example, consider a very large increase in relative humidity from 20% to 90% at 20°C (68°F). This would increase refractivity by ~70 N-units. In contrast, a very large temperature drop from 20°C to 0°C in completely dry air would only increase N by ~20 N-units.

The importance of water vapor gradient (de/dz) to RF propagation is often overlooked. Furthermore, although an immense amount of meteorological data are available in the public domain, very little of these data have sufficiently accurate de/dz for radar M&S applications. APL has developed several systems to measure meteorological data at a quality that is sufficient for radar M&S applications. These systems are routinely used to record meteorological data at Navy test events in order to support posttest reconstruction and analysis.

The primary system used to collect meteorological data is APL's Automated Environmental Assessment System (AEAS). AEAS continuously records meteorological data on the ship under test, including wind speed and direction, sky temperature, sea surface temperature, and air temperature, pressure, and humidity. The AEAS system also estimates and reports an evaporation duct height based on these measurements.

In addition to the sensors on board the ship, AEAS is capable of receiving data from two other APL systems, balloonsondes and rocketsondes. These sensors are typically launched from the ship under test to measure a vertical profile of the atmosphere above the evaporation duct, to capture surface-based ducting, and to characterize RF propagation in the upper atmosphere. The data measured by the sensors are streamed back to the AEAS system using an RF link and are recorded for posttest analysis. Over the past few years, APL has redesigned both AEAS and the rocketsonde sensor package used in the rocketsonde system. The new system has been in use since 2014 and has supported many of the recent Aegis Baseline 9, Standard Missile-6, and Ship-Self Defense System at-sea test events. A commercially available sensor package is used for the balloonsondes.

For some applications, a single vertical profile is insufficient to characterize the variation in the RF environment as a function of range and bearing. In these cases, APL's Helicopter Atmospheric Profiling System (HAPS) can be used to collect multiple profiles in the vicinity of the ship under test. The HAPS is currently being redesigned and will be provided to the Navy for at-sea test support. Figure 25 shows pictures of the various meteorological systems that have been developed at APL and are routinely used to support at-sea tests. For surface warfare (SUW) field tests, a commercial wave buoy system is used to characterize surface conditions.

Before the raw meteorological data can be used in radar M&S, it must undergo several quality control checks and postprocessing steps to obtain RF refractivity profiles that are well conditioned for RF propagation models. APL has developed the Multiple-source Assimilation and Refractivity Interpolator (MARI) software to process data from AEAS, rocketsondes, balloonsondes, and HAPS to characterize atmospheric refractivity for use by RF propagation models. These models are discussed next.

RF Propagation Models

APL's Tropospheric Electromagnetic Parabolic Equation Routine (TEMPER) software is widely regarded as the benchmark RF propagation model within the US Navy M&S community.[24] TEMPER is used for RF propagation analysis by over 400 users at more than 50 agencies, contractor sites, and universities. In addition to its large user base, TEMPER is distinguished from other RF propagation models by the amount of effort that has gone into validating it with measured data. Thus,
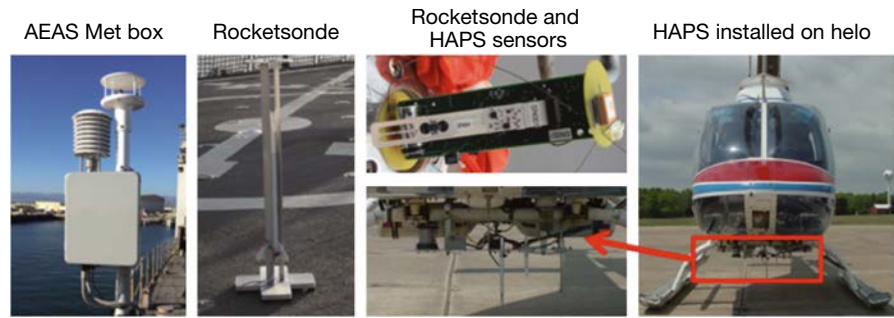
| AEAS Met box | Rocketsonde | Rocketsonde and HAPS sensors | HAPS installed on helo |

Figure 25. APL-developed meteorological measurement systems.

TEMPER has been accredited for use in a number of Navy programs.

TEMPER uses a Fourier-based, split-step algorithm to solve the two-dimensional parabolic equations, which are a simplified version of Maxwell's equations. The simplifying assumptions used in the derivation of TEMPER's formulation make it well suited for accurately predicting RF propagation in the low-elevation-angle region. Furthermore, TEMPER is numerically efficient with respect to other classes of electromagnetic solvers that provide similar accuracy.

One of the strengths of TEMPER is that the software can be used to predict RF propagation over a wide variety of propagation environments. A text input file is used to specify refractivity profiles to TEMPER. This allows arbitrary RF propagation environments to be input to TEMPER, whether they are based on modeled data or measured data. Similarly, terrain data can be specified to TEMPER through a text input file, allowing the effects of both land features and the ocean surface to be included in TEMPER's results.

The primary output of TEMPER is a complex propagation factor that is defined as the ratio of the electric field computed by TEMPER for a given set of environmental conditions to the electric field in free space. The propagation factor quantity is used within radar models to account for gains or losses due to the environment. Figure 26 shows TEMPER's propagation factor output for a 10-GHz transmitter for three different evaporation duct heights. The color scale in the plots indicates the strength of the field relative to free space propagation. The figure illustrates the variability in RF propagation due to environmental conditions. TEMPER's output also produces estimates of the grazing angle as a function of range. The propagation factor and grazing angle outputs are used within APL's land and sea clutter models.

TEMPER is typically used to model RF propagation for the anti-air warfare (AAW) and SUW missions because these missions usually involve detecting targets at low-elevation-angle geometries. For the BMD mission, targets are typically detected at higher elevation angles and longer ranges where multipath and refractive effects are not primary performance drivers for
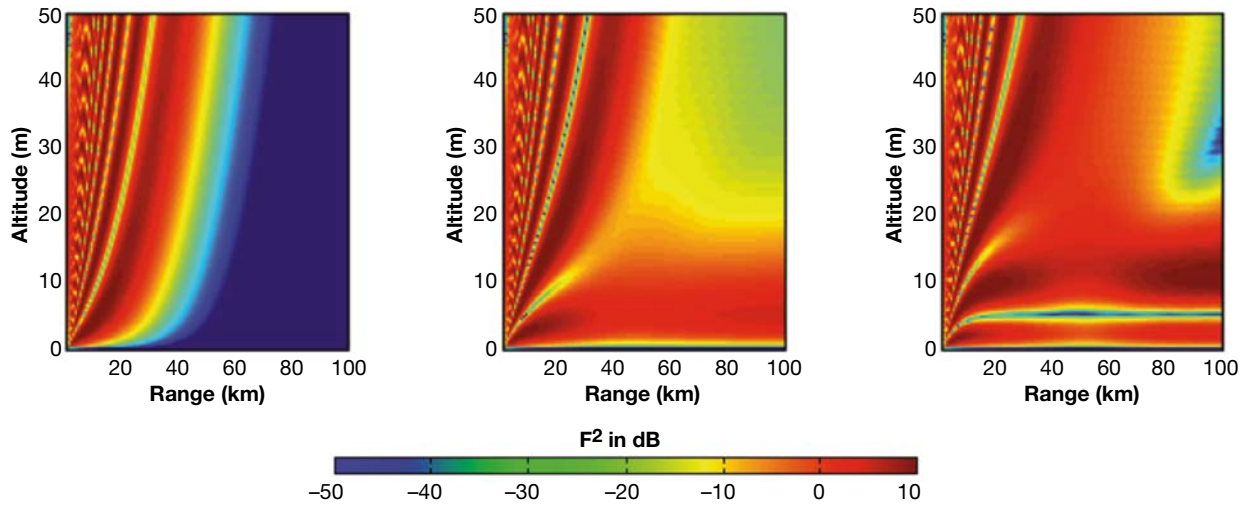
Figure 26. TEMPER propagation factor plots at 10 GHz for various evaporation ducts (left, 4 m; middle, 14 m; right 24 m).

the radar. Although TEMPER could be used for these types of calculations, alternative techniques are better suited because they provide the required accuracy with increased numerical efficiency.

APL's JAVA-based Ray tracing Computer Analysis Program (jRayCAP) is a first-principles ray tracing code that solves the full ray optics equations in two dimensions (range and height), allowing for range-varying refractivity profiles. Like TEMPER, jRayCAP can accept arbitrary refractivity and terrain profiles through its input files, making it a powerful tool for predicting RF propagation. The primary outputs from jRayCAP are lens loss, grazing angles, and estimates of refraction-induced range, altitude, and elevation angle biases.

System-Level Radar M&S

Figure 27 shows a high-level overview of how physics-based modeling of the natural environment can be used within radar M&S. A scenario is first defined by specifying the target data, environmental inputs, and properties of the radar. In this example, the scenario inputs are used to precompute RF propagation data using TEMPER and jRayCAP. Precomputation is often used because computing RF propagation data "in the loop" in the radar simulation is too slow. Furthermore, for scenarios where the target-to-radar geometry is known a priori, one can precompute the propagation data along the trajectory and only save these data, thus reducing the amount of storage that is required.

In cases where the target-to-radar geometry is not fully

defined by the scenario inputs (for example, reactive threats), a large set of precomputed propagation data must be saved or the propagation model must run in the loop. The trade-off between storage and run time must be considered for these types of analysis.

The propagation data are used within various parts of the radar simulation as it runs. Propagation factor is typically used within the radar range equation to account for gains or losses due to the environment. This allows the effects of the environment on detection and tracking performance to be modeled. In cases where radar measurements are modeled, propagation factor can also be included in the measurement model to evaluate the effect on angle estimation techniques like monopulse. Refraction errors can also be used in a measurement model to include biases that are due to the environment. Clutter data can be used to evaluate the effect of the environment on waveform selection techniques and also to evaluate how clutter affects the radar's detection performance and ability to reject clutter.
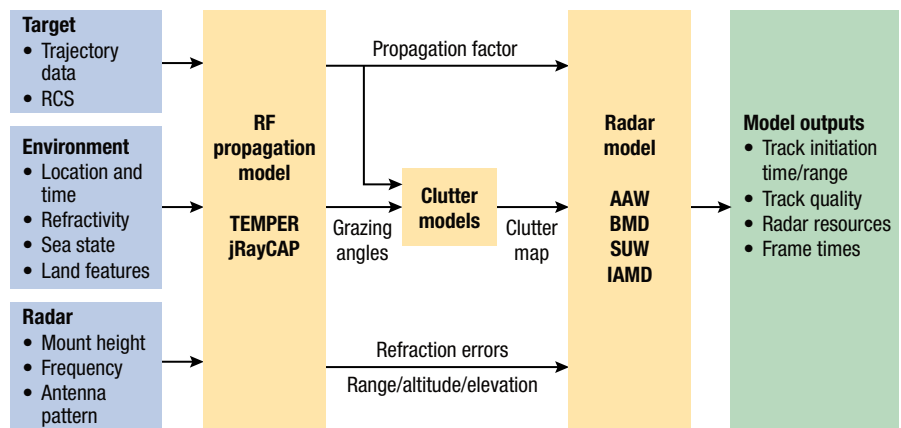

Figure 27. Overview of use of physics-based modeling in radar M&S. IAMD, integrated air and missile defense; RCS, radar cross section.

After the radar simulation is run, the outputs are analyzed to understand the performance of the radar for the scenario. Some of the key radar metrics may include track initiation time or range, measurement and track quality, radar resource usage, and search frame times. All these metrics are directly affected by the environment. Therefore, the performance of the radar can be characterized by varying the environmental inputs to the radar model.

Current Efforts

Because the environmental conditions can impose dramatic system-level effects on performance, it is important that the appropriate representative conditions be used. For pretest predictive assessments, these typically consist of climatological information representative of the geographical area of interest and the time of year. For short-term forecasting within a few days or hours of a test, APL has more recently been using Numerical Weather Prediction (NWP) model data, such as those generated by the US National Centers for Environmental Prediction or the US Navy's Fleet Numerical Meteorology and Oceanography Center. For posttest reconstruction, the measured meteorological data products described in the section titled M&S for Digital Phased-Array Radars are typically used, although often the NWP model data are used for inferring conditions downrange of the measured data or in cases where measured data were not collected.

Until recently, the majority of atmospheric climatological databases used within the radar testing and evaluation community drew on several-decades-old measured data of questionable quality that have sparse temporal and spatial resolution. These older databases have been oversimplified and do not provide statistics on the correlated nature of various phenomena. Newer and more numerous global observations using improved instrumentation have been used to drive NWP models that allow vastly improved spatial and temporal resolution. NWP model "reanalysis" data sets such as the US National Centers for Environmental Prediction Climate Forecast System Reanalysis and the European Centre for Medium-Range Weather Forecasts (ECMWF) Reanalysis-Interim (ERA-Interim) provide decades' worth of global coverage of the necessary data to assess RF propagation characteristics to at least a first order anywhere in the world at any time in the past three or more decades. Site-specific, correlated, range-dependent profiles of meteorological data can provide vastly improved fidelity to any analysis. Although these data can be down-sampled statistically based on percent occurrence, they also enable brute-force computations of full, multidecade, time-series data, sampled as often as hourly. Recent APL independent research and development has resulted in newly transformed reanalysis databases hosted on a 50-TB server at APL that allow for extraction of decades of time-corre-lated data from a single location in a matter of seconds. Although these data have primarily been used to support RF propagation analysis, the underlying data, such as temperature, precipitation, winds, ocean waves, and clouds, have been mined to answer other sponsor questions. For example, the four-dimensional wind speed and direction databases have been used for modeling drift of balloon-based systems.

Although numerical weather models hold a lot of promise as a source of data, they currently have many limitations. The vertical resolution of the models is typically insufficient to quantitatively assess the height and strength of any potential ducting layers. In coastal regions, the horizontal resolution of the models may not adequately resolve the difference between land and water or any topological features. These challenges, however, will be addressed by more powerful computing resources, along with increasing the quantity and quality of the observational data feeding the models. These efforts are currently well funded across the globe through research into climate change and a global demand for more accurate, longer-term weather forecasts. Validating the output of these models against measured data remains a priority, especially in regions of the world where the quality and quantity of weather observations is limited.

APL completed a significant update to TEMPER (v3.2) in September 2015, with the most notable enhancement being the new ocean surface generator mode that supports high-fidelity, physics-based SUW radar analysis. Another notable aspect of the v3.2 distribution is that, unlike previous versions, which could only run on Windows, v3.2 has been adapted to run on Linux and Mac operating systems as well as Windows.

APL is also building an easy-to-use application programming interface (API) around TEMPER called EMBER (Extensible Multi-domain Backbone for Environmental Representation), which encapsulates setting up and running TEMPER behind the API. EMBER is also being designed to use data caching and grid computing to address numerical efficiency for RF propagation calculations. One of the main goals is to allow M&S developers to more easily integrate TEMPER's capabilities. Although EMBER's initial API only supports SUW target modeling, EMBER's underlying design will accommodate a much broader range of capabilities to support radar M&S for the AAW and BMD missions. EMBER ultimately aims to provide consistent sensor-effects modeling across mission areas using various RF propagation models tailored to an end use.

Remote Sensing: Atmospheric Characterization and Correction for EO/IR Sensors and Systems

Over the past several years, the DoD community has renewed interest in understanding optical propagation in the maritime environment. A good understanding of the environment is important for predicting perfor-

mance of a variety of current and future EO/IR systems, including those used for optical intelligence, surveillance, and reconnaissance; HEL engagements; and FSO. Understanding the propagation effects for these types of systems from a US Navy platform proposes a unique set of challenges that need to be addressed before an exhaustive program of record is established. As technology moves forward, an area of focus for APL will be to assist the Navy with the performance assessment, calibration, and the design of such systems.

To date, atmospheric characterization is a key area where APL has supported many different sponsors in the DoD community. Because the atmosphere can be a highly variable environment where conditions can change within minutes, it is necessary to measure the atmospheric properties during the time of data collection. Standard products include band-integrated atmospheric transmittance and path radiance as a function of time for a given optical sensor or sensor band. These products are used to correct, calibrate, and normalize signatures obtained from optical sensors supporting numerous testing and evaluation programs.

Typically, APL fields a suite of ground-based instruments that includes two micropulsed lidars, a Fourier transform infrared (FTIR) spectroradiometer, particle sizers and particle counters, and a Cimel sun photometer (see Figure 28). Following a field campaign, the individual instrument results are fused together to develop

a total environmental picture for periods of time surrounding the test.

The FTIR unit passively collects IR radiation in both the mid- and long-IR wavelength regions. These data serve two important uses. First, the measurements themselves are used to provide calibrated, ground-based

Figure 28. Images of the FTIR (upper left), micropulsed lidars (lower), and sun photometer systems (upper right) used for atmospheric characterization.
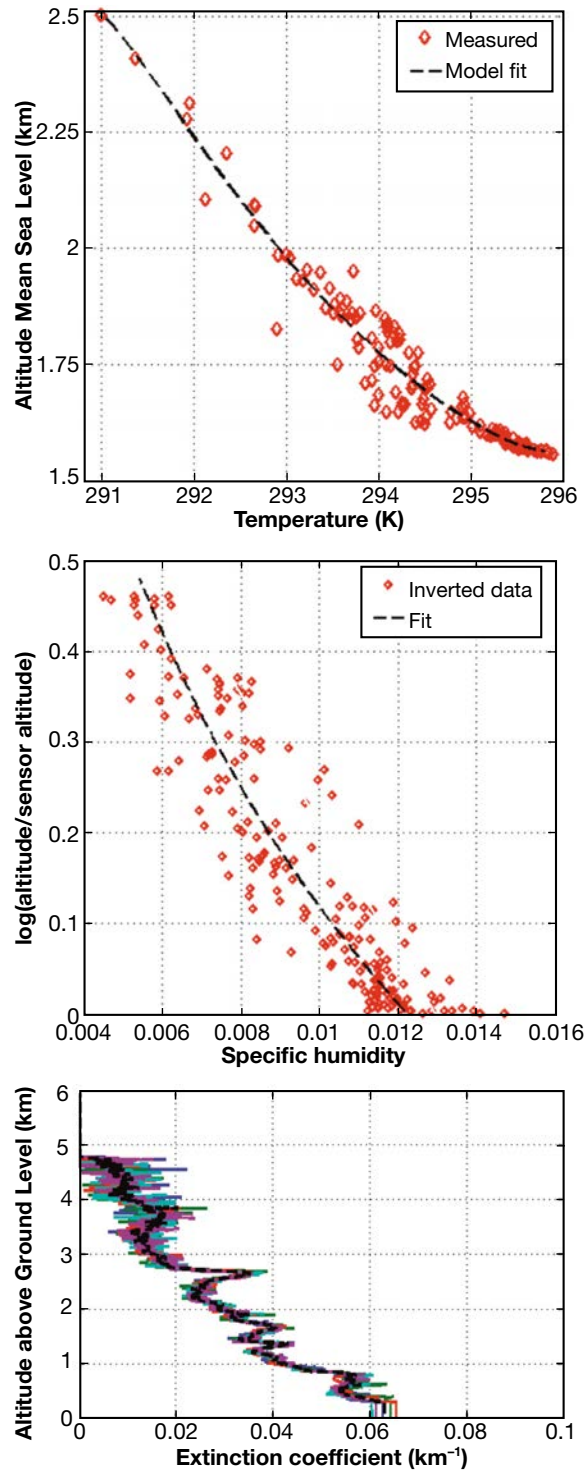

Figure 29. Example of temperature inversion (top), water vapor inversion (middle), and inverted 1047-nm lidar data using an averaged AOD of 0.14 to seed inversion (bottom).

radiance fluctuations and background levels to optical sensors. Second, these spectrally resolved radiance measurements are inverted via a multistep process[25,26] to provide profiles of water vapor, pressure, and temperature. An example of the inverted profiles for temperature and water vapor can be found in Figure 29 (top). Atmospheric extinction and scatter due to aerosols represents an additional metric that must be characterized. The Cimel sun photometer provides a measure of total aerosol optical depth (AOD), which represents a path-integrated value of the extinction. In comparison, the MPLs retrieve a range-resolved measure of backscattered photons, and the point sensors provide a ground-based measurement of aerosol loading. The real advantage comes in the co-location of the sun photometer, point sensors, and lidars, as each provides complementary information. When fused together, the result is a highly accurate picture of range-resolved extinction that is then constrained by the total AOD; see Figure 29 (bottom) for an example.[27,28]

The final step in the atmospheric characterization process is to combine the atmospheric profiles derived from the FTIR downwelling radiance measurements with the extinction measurements to create a set of user inputs to be used with a radiative transfer code, such as MODTRAN. When the atmospheric profile is used with MODTRAN, the radiance spectrum from the near infrared (NIR) to longwave infrared (LWIR) can be computed and verified with the original measured spectrum. This modeled spectrum can then be used to calculate transmission and background radiance for a given sensor spectral response along a line of sight as a function of time, as shown in Figure 30. These values enable APL engineers to calibrate collected data to obtain radiometric signatures.

Outside of performing optical characterization for T&E applications, APL engineers have developed new capabilities to help improve the community understanding of atmospheric turbulence, absorption, and scatter. These new competencies include both the development of simulation tools and the design and prototyping of instruments to fill gaps in existing capabilities. One of our key developments over the past several years was the creation of HELSIM, a sophisticated software tool that enables APL staff to numerically simulate the propagation of a laser beam through the atmosphere. Although the principal use of the tool is to assess performance of Navy HEL systems, it has also been used to guide the design and construction of turbulence characterization equipment. In addition to this cutting-edge work in numerical simulation of atmospheric propagation, APL staff have executed projects to further develop the Navy's understanding of atmospheric absorption at HEL-relevant wavelengths.

A key parameter that impacts the propagation of light through the atmosphere is turbulence. When performing numerical simulations, atmospheric turbulence is often expressed as pseudorandom phase screens spaced throughout the atmospheric path. Typically these screens are large grids of complex numbers. The size and sampling of these phase grids are often the limiting factor for numerical propagation simulations. Under IRAD funding, APL staff combined several different existing techniques for phase screen simulation to develop a new approach for incorporation into HELSIM. The result of the effort was a new way to endlessly generate phase screens on the fly for any given propagation geometry as a function of time. This new approach enables APL engineers to greatly reduce simulation artifacts occurring because of the looping of phase screens when performing HEL control-loop trade simulations. More recent HELSIM developments have included the incorporation of adaptive optics and the ability to simulate turbulence-degraded images. A few examples of these capabilities are shown in Figure 31.
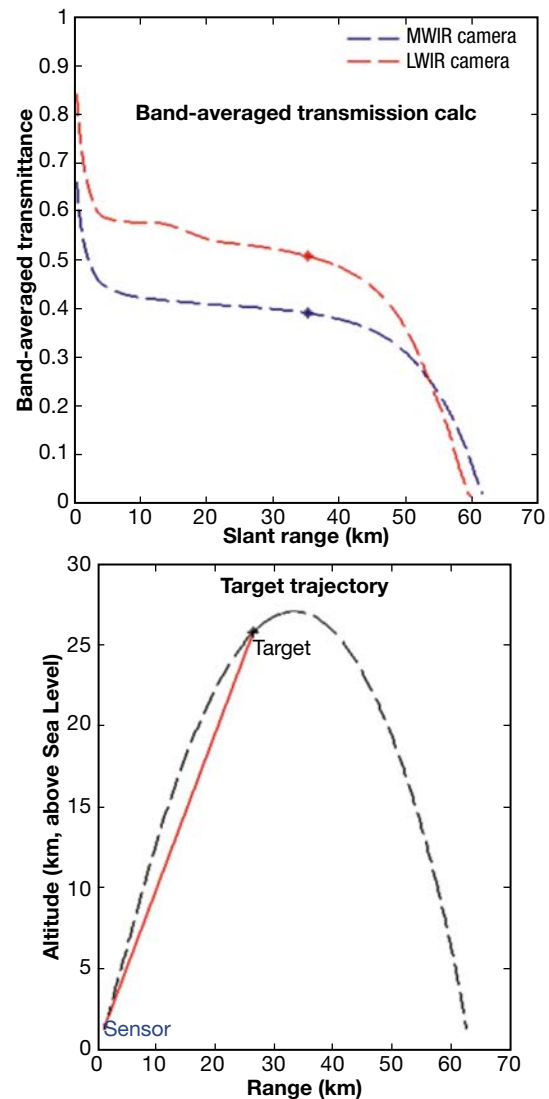

Figure 30. Example IR transmittance product as a function of slant range to target.
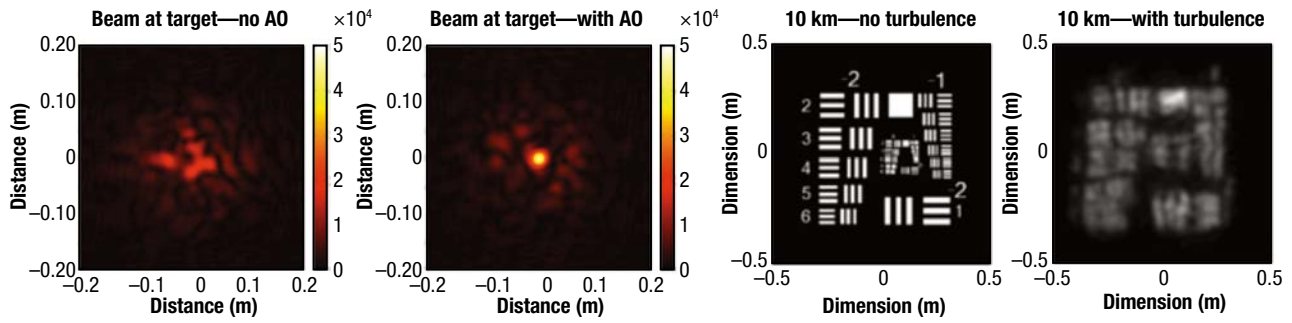
Figure 31. Example of a numerical simulation result with and without adaptive optics (AO; left) and with and without turbulence of an extended image (right).

HELSIM was also used to design and build a laser-based differential image motion monitor (DIMM).[29] This instrument was built to measure path-integrated turbulence along paths ranging from a few to tens of kilometers. The APL DIMM sensor has been fielded for a variety of tests in which it has been used to assess the performance of a variety of active and passive optical systems, such as EO/IR intelligence, surveillance, and reconnaissance and FSO. A simple system diagram and example data compared to a scintillometer measurement along the same path can be found in Figure 32.

An additional loss factor in the propagation of light through the atmosphere is the atomic absorption due to atmospheric water vapor and oxygen. Although absorption is often denoted as a secondary effect to the aerosol scattering, high-power levels of emerging laser technology require the consideration of absorption effects because of their impact on additional nonlinear losses, such as thermal blooming.

Absorption can vary greatly depending on the wavelength of light being used (see Figure 33, left), where the atmospheric absorption coefficient in the NIR is shown on a logarithmic scale. Note that a laser spectrally overlapping a local water vapor line can have an absorption coefficient an order of magnitude stronger than adjacent wavelength location where the absorption would be dictated by the continuum band beneath the local lines. This continuum absorption has two sources, the water vapor continuum and molecular oxygen collision-induced absorption (CIA). Recent studies[30] at APL have been conducted to carefully characterize this CIA band to assess its potential impact to HEL systems. To explore these (relatively) weak oxygen CIA bands at NIR wavelengths, APL engineers performed a series of high-resolution laboratory measurements as a function of pressure, temperature, and nitrogen-oxygen mixture ratios. The measurements were taken at elevated pressure in a 300-m white cell in order to accentuate the CIA bands. Following the measurements, a line-by-line model was developed and used with the measured results to develop an in-depth understanding of these CIA bands. A comparison of the APL results to the MODTRAN 4/5 absorption coefficient is made in Figure 33 (right). The APL result shows a notable increase in the absorption coefficient over what is currently incorporated in the industry standard MODTRAN 4/5 tool. APL engineers have worked over the past few years to share these results with the community to help to further improve the MODTRAN tool for future versions.
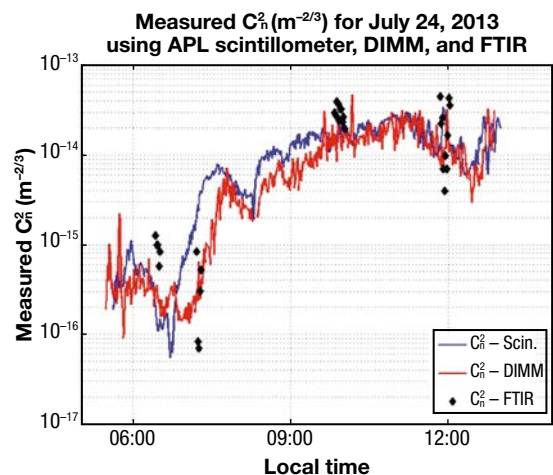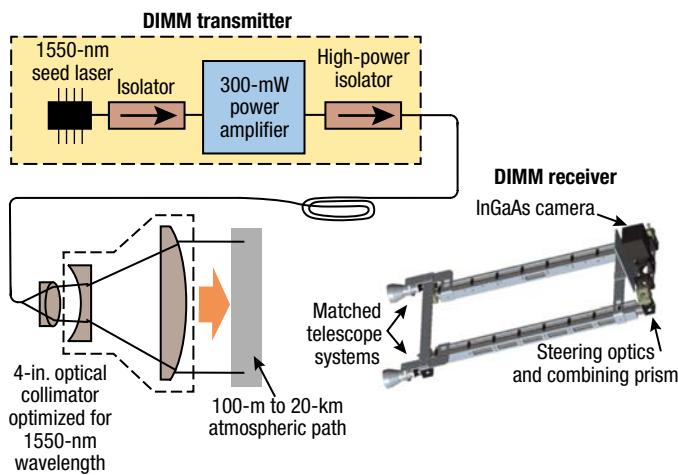

Figure 32. APL DIMM system diagram (left) and example data product (right).
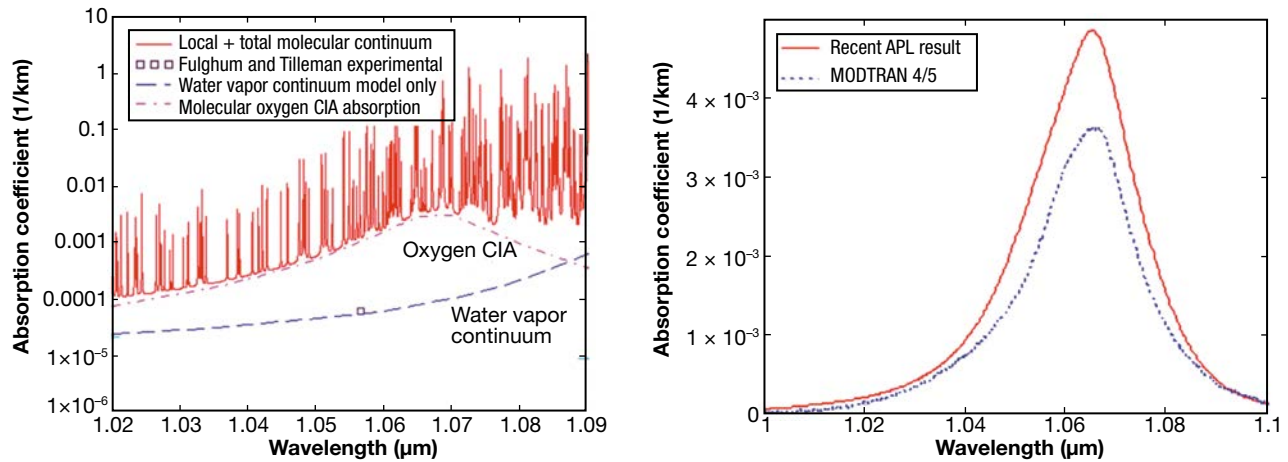
Figure 33. Atmospheric absorption at NIR wavelengths (left) and APL continuum result compared to MODTRAN 4/5 (right).

REFERENCES

[1]K. O'Haver, C. Barker, G. D. Dockery, and J. D. Huffaker, "Radar Development for Air and Missile Defense," *Johns Hopkins APL Tech. Dig.*, vol. 34, no. 2, pp. 140–153, 2018.

[2]S. H. Talisa, K. W. O'Haver, T. M. Comberiate, M. D. Sharp, and O. F. Somerlock, "Benefits of digital phased array radars," *Proc. IEEE*, vol. 104, no. 3, pp. 530–543, 2016.

[3]G. Fein, "DARPA effort to alter future AESA radar use," *Int. Defence Review*, Sept. 15 2014, Weapons and Equipment Section, United States.

[4]S. Bhatia, W. M. Dorsey, J. Glancy, C. B. Huber, M. Luesse, K. O'Haver, et al., "Measurement techniques for a transmit/receive digital phased array," in *Proc. 2011 Antenna Measurement and Techniques Association Conf.*, Englewood, CO, 2011.

[5]M. T. Ho, H. A. Krichene, G. F. Ricciardi, and W. J. Geckle, "A computationally-efficient, CRLB-achieving range estimation algorithm," in *Proc. 2015 IEEE Radar Conf.*, Arlington, VA, pp. 0005–0010, May 2015.

[6]H. A. Krichene, M. J. Pekala, M. D. Sharp, K. C. Lauritzen, D. G. Lucarelli, and I.-J. Wang, "Compressive sensing and stretch processing," in *Proc. 2011 IEEE Radar Conf.*, Kansas City, MO, pp. 362–367, May 2011.

[7]I. Ilhan, A. C. Gurbuz, and O. Arikan, "Sparsity based robust stretch processing," *Proc. 2015 IEEE Int. Conf. on Digital Signal Processing*, Singapore, pp. 95–99, Jul. 2015.

[8]G. F. Ricciardi, J. R. Connelly, H. A. Krichene, and M. T. Ho, "A fast-performing error simulation of wideband radiation patterns for large planar phased arrays with overlapping subarray architecture," *IEEE Trans. Antenn. Propag.*, vol. 62, no. 4, pp. 1779–1788, 2014.

[9]M. A. Richards, *Fundamentals of Radar Signal Processing*, 2nd ed. New York: McGraw-Hill, 2014.

[10]D. A. Day, "Robust phase-only nulling for adaptive and non-adaptive phased arrays," in *Proc. Asilomar Conf. on Signals, Systems, and Computers*, Pacific Grove, CA, pp. 2173–2176, Nov. 2007.

[11]H. A. Krichene, M. T. Ho, S. H. Talisa, G. F. Ricciardi, and K. C. Lauritzen, "Effects of channel mismatch and phase noise on jamming cancellation," in *Proc. 2014 IEEE Radar Conf.*, Cincinnati, OH, pp. 0038–0043, May 2014.

[12]H. A. Krichene, M. T. Ho, M. D. Sharp, and S. H. Talisa, "Effects of third-order intermodulation on jamming cancellation," in *Proc. 2015 IEEE Radar Conf.*, Arlington, VA, May 2015.

[13]H. A. Krichene, "Generation of range-time intensity (RTI) plots of BMD events," in *Proc. 2009 Tri-Service Radar Symp.*, Boulder, CO.

[14]H. A. Krichene, M. T. Ho, and G. F. Ricciardi, "Performance assessment of sidelobe jamming cancellation using stretch processing," in *Proc. 2015 Int. Radar Symp.*, Dresden, Germany, pp. 102–107 (Jun. 2015).

[15]P. W. Juodawlkis, J. J. Hargreaves, R. D. Younger, G. W. Titi, and J. C. Twichell, "Optical down-sampling of wide-band microwave signals," *J. Lightwave Technol.*, vol. 21, no. 12, pp. 3116–3124, 2003.

[16]J. Kim, M. J. Park, M. H. Perrott, and F. X. Kärtner, "Photonic subsampling analog-to-digital conversion of microwave signals at 40-GHz with higher than 7-ENOB resolution," *Opt. Express*, vol. 16, no. 21, pp. 16509–16515, Oct. 13, 2008.

[17]M. B. Airola, S. R. O'Connor, M. L. Dennis, and T. R. Clark, "Experimental demonstration of a photonic analog-to-digital converter architecture with pseudorandom sampling," *IEEE Photonics Technol. Lett.*, vol. 20, no. 24, pp. 2171–2173, 2008.

[18]P. Feng and Y. Bresler, "Spectrum-blind minimum-rate sampling and reconstruction of multi-band signals," in *Proc. IEEE Int. Conf. on Acoustics Speech, and Signal Processing*, Atlanta, GA, pp. 1688–1691, 1996.

[19]C. Herley and P. W. Wong, "Minimum rate sampling and reconstruction of signals with arbitrary frequency support," *IEEE Trans. Inf. Theory*, vol. 45, no. 5, pp. 1555–1564, 1999.

[20]E. J. Candes, J. Romberg, and T. Tao, "Robust uncertainty principles: exact signal reconstruction from highly incomplete frequency information," *IEEE Trans. Inf. Theory*, vol. 52, no. 2, pp. 489–509, 2006.

[21]M. Mishali and Y. C. Eldar, "From theory to practice: Sub-Nyquist sampling of sparse wideband analog signals," *IEEE J. Sel. Top. Signal Process.*, vol. 4, no. 2, pp. 375–391, 2010.

[22]I. Bilinskis and A. Mikelsons, *Randomized Signal Processing*. Hemel Hempstead, Hertfordshire: Prentice-Hall, 1992.

[23]S. F. Cotter, B. D. Rao, K. Engan, and K. Kreutz-Delgado, "Sparse solutions to linear inverse problems with multiple measurement vectors," *IEEE Trans. Signal Process.*, vol. 53, no. 7, pp. 2477–2488, 2005.

[24]G. D. Dockery, R. S. Awadallah, D. E. Freund, J. Z. Gehman, and M. H. Newkirk, "An overview of recent advances for the TEMPER radar propagation model," in *Proc. 2007 IEEE Radar Conf.*, Boston, MA, pp. 896–905, Apr. 2007.

[25]M. E. Thomas and M. D. Banta, "Passive remote sensing of the atmosphere by a ground based spectroradiometer," in *Proc. Int. Geoscience and Remote Sensing Symp.*, 2000.

[26]A. K. Lazarevich, M. E. Thomas, C. R. Philbrick, and R. I. Joseph, "Survey of atmospheric remote sensing techniques leveraging information in passive IR spectral radiance measurements," in *2004 IEEE Int. Geoscience and Remote Sensing Symp. Proc.*, Anchorage, AK, pp. 4769–4772, Sept. 2004.

[27]A. M. Brown, M. B. Airola, D. M. Brown, M. Keller, C. M. Martin, et al., "Hydrosol characterization in maritime environments," in *Proc. 35th Review of Atmospheric Transmission Models Meeting*, 2014.

[28]S. B. Strong and A. M. Brown, "Developing a broad spectrum atmospheric aerosol characterization for remote sensing platforms over desert regions," in *Infrared Imaging Systems: Design, Analysis, Modeling, and Testing XXV, Proc. SPIE*, vol. 9071, G. C. Holst, K. A. Krapels, G. H. Ballard, J. A. Buford, and R. L. Murrer, Eds., SPIE, Bellingham, WA, 907115, Jun. 9, 2014.

[29]D. M. Brown, J. C. Juarez, and A. M. Brown, "Laser differential image-motion monitor for characterization of turbulence during free-space optical communication tests," *Appl. Opt.*, vol. 52, no. 34, pp. 8402–8410, Dec. 1, 2013.

[30]M. E. Thomas and D. M. Brown, "Near-infrared continuum absorption by water vapor and oxygen," in *Proc. 2010 Atmospheric Transmission Meeting*, Lexington, MA, 2010.

James D. Huffaker, Air and Missile Defense Sector, Johns Hopkins University Applied Physics Laboratory, Laurel, MD

James Dodd Huffaker is a Principal Professional Staff member and assistant supervisor of the Sensor and Communication Systems Branch in APL's Air and Missile Defense Sector. He received a BS and an MS in electrical engineering, both from Georgia Tech. He has 30 years' experience in advanced radar system development, analysis, testing, and simulation for the US Navy and Missile Defense Agency, primarily focused on AN/TPY-2, Aegis AN/SPY-1, and AN/SPY-6. His email address is dodd.huffaker@jhuapl.edu.

Christopher K. Barker, Air and Missile Defense Sector, Johns Hopkins University Applied Physics Laboratory, Laurel, MD

Christopher Barker is a Principal Professional Staff member and program manager in APL's Air and Missile Defense Sector. He received a BS in political science from the United States Naval Academy and served as a commissioned officer and carrier aviator in the E-2C Hawkeye community. Since joining APL in 2009, he has managed the Air and Missile Defense Radar (AMDR) program and other related advanced Surface Navy radar development initiatives. In 2014, he and teammates were granted the APL Achievement Award for Outstanding Mission Accomplishment for their contributions to AMDR capabilities. His email address is christopher.k.barker@jhuapl.edu.

David M. Brown, Air and Missile Defense Sector, Johns Hopkins University Applied Physics Laboratory, Laurel, MD

David Brown is a Principal Professional Staff member and supervisor of the High Energy Laser Systems and Technology Section in APL's Air and Missile Defense Sector. He received BS, MS, and PhD degrees in electrical engineering from Pennsylvania State University. He has an extensive background in electrical and optical engineering, with experience and interests in high-energy laser (HEL) systems, atmospheric propagation, and optical sensing. He has supported a wide variety of projects that pertain to the development of high-energy fiber lasers and is the principal investigator for a task to develop advanced modulation schemes for stimulated Brillouin scattering mitigation in these systems. Dr. Brown serves as a subject matter expert for development and fielding of active and passive remote sensing systems for a variety of DoD applications, including the advancement of specialized types of laser and lidar systems for characterization of atmospheric turbulence, scattering, and absorption. He has a strong track record in leading technical projects with participants from both DoD and academia. His email address is david.m.brown@jhuapl.edu.

Donald E. Chesley, Air and Missile Defense Sector, Johns Hopkins University Applied Physics Laboratory, Laurel, MD

Donald E. Chesley is a chief engineer and Principal Professional Staff member in APL's Air and Missile Defense Sector. He earned a BS in electrical engineering from Rutgers University and an MS in electrical engineering from Drexel University. He has extensive experience in research and development of advanced radar systems for Navy and other DoD applications. When working in industry, he was involved in key new radar initiatives, defining system-level architectures to meet a broad range of operational requirements. His primary emphasis was on shipboard fire control radars, with missions including surveillance, tracking, and engagement of anti-ship cruise missiles, ballistic missiles, and airborne threats in severe clutter and jamming environments. During his work at APL, he has continued and broadened this experience, applying expertise in support of radar development for Navy program offices, holding several senior leadership roles both within APL and in external Navy technical organizations. His email address is donald.chesley@jhuapl.edu.

Thomas R. Clark Jr., Air and Missile Defense Sector, Johns Hopkins University Applied Physics Laboratory, Laurel, MD

Thomas R. Clark Jr. is a Principal Professional Staff member and supervisor of the Optics and Photonics Group in APL's Air and Missile Defense Sector. He received a BS in physics from Loyola College (now Loyola University) in Maryland, an MS in physics from Lehigh University, and a PhD in physics from the University of Maryland, College Park. He previously held positions as a research physicist in the Optical Sciences Division at the Naval Research Laboratory; as a senior optical design engineer at the venture-backed Dorsal Networks, later acquired by Corvis Corporation; and as director of photonics at Pharad, LLC. His research interests include the study of lasers and nonlinear optics, the development and characterization of low-noise and ultrafast photonic systems and devices, and the application of photonics to problems in optical communications and microwave and millimeter-wave systems. Dr. Clark is a member of the IEEE Photonics Society, the IEEE Microwave Theory and Techniques Society, and OSA (The Optical Society). He has chaired and served on the committees for many technical conferences. His email address is thomas.clark@jhuapl.edu.

G. Daniel Dockery, Air and Missile Defense Sector, Johns Hopkins University Applied Physics Laboratory, Laurel, MD

G. Daniel Dockery is a Principal Professional Staff member and supervisor of the Sensor and Communication Systems Branch in APL's Air and Missile Defense Sector. He received a BS in physics and an MS in electrical engineering, both from Virginia Tech. He completed coursework in the University of Maryland's PhD program in electrical engineering. Since joining APL in 1983,

Dan has worked in the areas of EM propagation and radar engineering as well as environmental characterization for US Navy radar and communication systems. His email address is dan.dockery@jhuapl.edu.

Charles L. Farthing, Air and Missile Defense Sector, Johns Hopkins University Applied Physics Laboratory, Laurel, MD

Charles Farthing is a Principal Professional Staff member in APL's Air and Missile Defense Sector. He received a BS in electrical engineering from Virginia Tech and an MS in applied physics from Johns Hopkins University. His experience spans the fields of radar system design and performance analysis, ballistic missile defense, aircraft and missile systems, test and evaluation, and electromagnetic compatibility/vulnerability. Mr. Farthing has extensive experience with the Aegis Weapon System and AN/SPY-1 radar variants, including AN/SPY-1D(V), as well as with the DDG 1000 Dual Band Radar (DBR). His radar systems engineering experience covers the area between solving very specific problems at the signal processor level to analyzing performance impact of design choices on overall weapon system performance. He currently spends most of his time working on the Air and Missile Defense Radar (AMDR) S-band functional architecture and leading requirements development for the AMDR Radar Suite Specification. He teaches radar system engineering for the Johns Hopkins University Engineering for Professionals program. His email address is charles.farthing@jhuapl.edu.

Khadir A. Griffith, Air and Missile Defense Sector, Johns Hopkins University Applied Physics Laboratory, Laurel, MD

Khadir A. Griffith is a Senior Professional Staff member, radar engineer, and supervisor of the EM Propagation Modeling & Analysis Section in APL's Air and Missile Defense Sector. He obtained his master's degree in electrical and computer engineering from Ohio State University. In 2015, he received one of the Black Engineer of the Year Awards during an event held by the organization's annual Science, Technology, Engineering and Math Global Competitiveness Conference in Washington, DC. He was recognized with the Science Spectrum Trailblazer award, given to men and women actively creating new paths for others in science, research, technology, and development. While he was a graduate student at Ohio State's ElectroScience Laboratory, Khadir received the Best Paper Award at the 2008 Position Location and Navigation Symposium (PLANS) for his paper titled "Effect of Mutual Coupling on the Performance of GPS AJ Antennas." His email address is khadir.griffith@jhuapl.edu.

Minhtri T. Ho, Air and Missile Defense Sector, Johns Hopkins University Applied Physics Laboratory, Laurel, MD

Minhtri Ho, a radar engineer and analyst, is a Senior Professional Staff member and supervisor of the Advanced Signal Processing Section in APL's Air and Missile Defense Sector. He received a BS in electrical engineering from the University of Maryland, College Park, and an MS and a PhD in electrical engineering from Northeastern University. He works in the fields of radar signal processing, systems engineering, and data analysis and has a strong background in mathematics and sciences. He is an adjunct faculty member in the Mathematics/Statistics program at the University of Maryland University College. His email address is minhtri.ho@jhuapl.edu.

Shaun T. Hutton, Asymmetric Operations Sector, Johns Hopkins University Applied Physics Laboratory, Laurel, MD

Shaun T. Hutton is a chief engineer in APL's Asymmetric Operations Sector. He holds a BS in computer science from Baylor University, an MS in computer science from the University of Virginia, and an MDiv from the Southern Baptist Theological Seminary. His experience includes cybersecurity systems engineering as well as developing and applying the mission-based analysis (MBA) methodology on various space and naval systems. He is experienced with Navy combat systems and cyber domain. Other skill areas include trusted computing, network security, systems engineering, and software design and development. His email address is shaun.hutton@jhuapl.edu.

Juan C. Juarez, Air and Missile Defense Sector, Johns Hopkins University Applied Physics Laboratory, Laurel, MD

Juan C. Juarez was a member of the Senior Professional Staff and the lead engineer for FSO Communications in APL's Air and Missile Defense Sector. Under the FOENEX program, he led the development of the FSO communications system. He also led ongoing lasercom efforts, including development of compact, high-rate lasercom systems for mobile platforms.

Hedi A. Krichene, Air and Missile Defense Sector, Johns Hopkins University Applied Physics Laboratory, Laurel, MD

Hedi A. Krichene is a senior adaptive array/radar systems engineer in APL's Air and Missile Defense Sector. He received a BS in electrical engineering from Virginia Tech, an MS in electrical engineering from the University of Illinois at Urbana-Champaign, and an MS in mathematics/applied math from Johns Hopkins University. He has extensive experience in adaptive digital beamforming and

wideband/stretch radar signal processing. He has worked on various projects assessing electronic protection requirements and techniques. In addition, he is the principal investigator of an independent research and development project to investigate the use of game-theoretic and Markov decision processes into performance analysis of anti-air warfare and ballistic missile defense combat systems. He has twice won APL's R. W. Hart Prize in recognition of independent research and development efforts (in 2007 and honorable mention in 2010). His email address is hedi.krichene@jhuapl.edu.

Joseph N. Mulé, Air and Missile Defense Sector, Johns Hopkins University Applied Physics Laboratory, Laurel, MD

Joseph N. Mulé is a Principal Professional Staff member and chief engineer in APL's Air and Missile Defense Sector. He received a BS in aerospace engineering and an MS in mechanical engineering from the State University of New York. He has over 24 years of experience in the test and evaluation of ballistic missile defense weapon systems. His comprehensive experience includes the development of test objectives and requirements, flight test scenario design and development, launch systems engineering, and the conduct of flight tests and experiments. Mr. Mulé is an experienced launch vehicle systems engineer and has provided technical leadership and management for a variety of launch vehicles and payloads used as targets for intercept testing and tracking exercises. He has held key positions in a wide variety of BMD testing programs and has interfaced with several test ranges. His email address is joe.mule@jhuapl.edu.

Kenneth W. O'Haver, Air and Missile Defense Sector, Johns Hopkins University Applied Physics Laboratory, Laurel, MD

Kenneth O'Haver is a Principal Professional Staff member and chief scientist in the Sensor and Communications Branch in APL's Air and Missile Defense Sector. He received a BS in electrical engineering from Virginia Tech and an MS in electrical engineering from Johns Hopkins University. He has over 30 years of experience in the development of advanced radar systems, communications systems, electronic warfare systems, phased-array antennas, and advanced RF technologies. He has published numerous technical papers and has presented at various conferences. His email address is ken.ohaver@jhuapl.edu.

Shawn A. Phillips, Air and Missile Defense Sector, Johns Hopkins University Applied Physics Laboratory, Laurel, MD

Shawn A. Phillips is a Principal Professional Staff member, project manager, and assistant supervisor of the Radar and Electronic Warfare Systems Development Group in APL's Air and Missile Defense Sector. He earned a BS in physics from Youngstown State University, an MS in electrical and computer engineering from Northwestern University, and a PhD in electrical engineering from the University of Washington. He is a multidisciplinary digital systems engineer with extensive experience in the research and development of real-time high-performance computing systems using embedded software and firmware running on field-programmable gate arrays, graphics processing units, and general-purpose processors. His has served as an individual contributor and technical lead in defining and developing real-time systems in the signals intelligence, communication, and radar domains, as well as the information assurance and anti-tamper domains. His email address is shawn.phillips@jhuapl.edu.

Gerald F. Ricciardi, Air and Missile Defense Sector, Johns Hopkins University Applied Physics Laboratory, Laurel, MD

Gerald F. Ricciardi is a Principal Professional Staff member and assistant group supervisor in APL's Air and Missile Defense Sector. He received a BS in electrical engineering from Columbia University, an MS in electrical engineering from Johns Hopkins University, and a PhD in electrical engineering from Virginia Tech. He is experienced in phased arrays, radar, computational electromagnetics, RF scattering, polarization, calibration, algorithm development for various sensor-based applications, and modeling and simulation. He has directed science and technology efforts as the principal investigator of a Phase II Small Business Innovation Research (SBIR) program sponsored by the Missile Defense Agency in ballistic missile defense discrimination. Dr. Ricciardi has frequently served as a subject matter expert and technical analyst to render design, test, and performance recommendations. His email address is gerald.ricciardi@jhuapl.edu.

Salvador H. Talisa, Air and Missile Defense Sector, Johns Hopkins University Applied Physics Laboratory, Laurel, MD

Salvador H. Talisa is in APL's Radar and Electronic Warfare Systems Development Group, where he is a member of the Principal Professional Staff and a chief scientist. He received a telecommunications engineering degree from the Polytechnic University of Catalonia, Barcelona, Spain, and an MSc and a PhD in electrical engineering from Brown University. He then joined the Westinghouse (later Northrop Grumman) Science and Technology Center, where he worked on microwave magnetic, magneto-optic, and microwave superconducting devices and materials. In 1997, he transferred to the Northrop Grumman Electronic Sensors and Systems near Baltimore, where he was a program and business development manager for receiver and exciter technology. His work currently focuses on digital array radar technology and on the support of various Defense Advanced Research Projects Agency (DARPA), Office of Naval Research (ONR), and US Navy advanced surface radar projects. He has authored and coauthored more than 50 articles and has been awarded seven patents. His email address is salvador.talisa@jhuapl.edu.